International Journal of Thermal Sciences 148 (2020) 106160

Contents lists available at ScienceDirect

International Journal of Thermal Sciences

journal homepage: www.elsevier.com/locate/ijts

Thermo-solute natural convection with heat and mass lines in a uniformly heated and soluted rectangular enclosure for low Prandtl number fluids

Durgesh Kushawaha [a], Sushil Yadav [b], Dwesh K. Singh [c,*]

[a] Department of Mathematics, Faculty of Mathematical Sciences, University of Delhi, Delhi, India
[b] Department of Mathematics, Maharaja Agrasen College, University of Delhi, Delhi, India
[c] Department of Mechanical Engineering, Dr. B. R. Ambedkar National Institute of Technology, Jalandhar, India

ARTICLE INFO

MSC:
35Q307
76D05
76M12
80A20

Keywords:
Combined heat and solute transfer
Finite difference
Streamline-vorticity formulation
Nusselt and Sherwood numbers
Buoyancy ratio effect
Heatlines & masslines

ABSTRACT

Thermo-solute natural convection with heat and mass lines in a uniformly heated and soluted rectangular enclosure for low Prandtl number fluids is studied. The left and right walls are maintained at constant temperature and solute while the bottom and top walls are adiabatic and non-diffusive. The finite difference method, together with the successive over-relaxation (SOR) technique, is used to solve the flow governing equations after converted into the vorticity-stream function form. Heat and mass lines visualization techniques are used for the better visualization of energy and solute distribution in the enclosure. The results obtained in this study are compared with experimental and numerical those from literature and found to be in good agreement. The influence of Rayleigh number $(\mathrm{Ra} = 10^3, 10^4, 10^5)$, Prandtl number $(\mathrm{Pr} = 0.015, 0.025, 0.71)$, Lewis number $(\mathrm{Le} = 1, 2, 5)$, and Buoyancy ratio $(\mathrm{N} = -1, 0, 1)$ on streamlines, isotherms, isosolutes, heatlines, masslines, total heat and mass transfer are examined. The parameters mentioned above considerably influence the total heat and solute transfer rates; moreover, the heat and mass lines play significant roles in understanding the distribution of energy and solute transfers in the enclosure.

1. Introduction

The thermo-solute natural convection is a process of buoyancy driven flows induced by the combined temperature and solute gradients. Alternatively, the buoyancy force is developed by combined concentration and temperature gradients. Technical applications of this type of thermo-solute natural convection process are e.g., geophysics [1,2], solar collector [3], drying technology [4], food engineering [5], biomechanics [6], distillation [7], and building engineering [8]. Rectangular enclosures are widely employed in many industries. Examples include tank storage, energy transfer devices, reactor systems, solar collectors, and engine cooling systems. Liquid metals are characterized by a very low Prandtl number due to their very high heat diffusivity. Pr = 0.015 and Pr = 0.025 represent liquid mercury and liquid gallium respectively. Liquid metals are considered in many nuclear and non-nuclear processes. In the frame of the future generation of nuclear reactors, liquid metals are foreseen to be used as a primary coolant. In the non-nuclear energy generation, liquid metals are used as a heat transfer medium in solar plants, where the sunlight is reflected by numerous mirrors onto a heat exchanger operated with liquid metals.

Natural convection in three-dimensional rectangular enclosures utilizing a very low Prandtl number fluid (Pr = 0.008) has been investigated by Crunkleton et al. [9]. The influence of Rayleigh number and aspect ratio on flow structures and heat transfer have been discussed in detail. Zhang and his group members have been done some good works on low Prandtl number fluids. Effect of surface heat dissipation, flow pattern transition, and destabilization mechanism on thermocapillary convection for low Prandtl number fluids in shallow and deep annular pools have been analyzed in [10–12]. Xu and his group (Xu et al. [13]; Yu et al. [14]) studied transient natural convective heat transfer of a low Prandtl number fluid from a heated horizontal circular cylinder to its coaxial and inner coaxial triangular enclosures. Flow structures and heat transfer in different types of geometries utilizing low Prandtl number fluids have considered in [15–17]. Deshmukh et al. [18] investigated the natural convection in different aspect ratios cavities utilizing moderate Prandtl number fluid. Zhang et al. [19] have investigated double-diffusive Rayleigh–Bénard convection of a moderate Prandtl number binary mixture in cylindrical enclosures. On recent application, Liu and his group (Ma and Liu [20]; Ge et al. [21]) developed novel applications using liquid metals for cooling of electronic chips and high power devices.

* Corresponding author.
E-mail addresses: durgeshoct@gmail.com (D. Kushawaha), syadav@mac.du.ac.in (S. Yadav), singhdk@nitj.ac.in (D.K. Singh).

https://doi.org/10.1016/j.ijthermalsci.2019.106160
Received 29 April 2019; Received in revised form 22 October 2019; Accepted 25 October 2019
1290-0729/© 2019 Elsevier Masson SAS. All rights reserved.

Nomenclature

D	mass diffusivity, m^2/s
H	dimensionless heat function
L	inclosure length
M	dimensionless mass function
P	dimensionless pressure
S	dimensionless solute
S^*	solute
T	dimensionless temperature
T^*	temperature, K
U, V	dimensionless velocities in X- and Y-direction
X, Y	dimensionless cartesian coordinates
Le	lewis number
N	buoyancy ratio
Sh	local Sherwood number
Sh_{avg}	average Nusselt number
Pr	Prandtl number
Ra	Rayleigh number
Nu	local Nusselt number
Nu_{avg}	average Nusselt number
g	gravitational acceleration, m/s^2
h	heat function
m	mass function
p	pressure, Pa
t	time
u, v	velocities components in x-, y-direction, m/s
x, y	cartesian coordinates

Greek Symbols

α	thermal diffusivity, m^2/s
β_{S^*}	coefficient of solute expansion, m^3 kg
β_{T^*}	coefficient of thermal expansion, K^{-1}
μ	dynamic viscosity, kg/ms
ν	kinematic viscosity, m^2/s
Ω	non-dimensional vorticity function
ω	dimensional vorticity function
Ψ	non-dimensional stream function
ψ	dimensional stream function
ρ	fluid density, kg/m^3
τ	non-dimensional time
c_p	specific heat at constant temperature
k	thermal conductivity

Subscripts

h	higher
l	lower
max	maximum
min	minimum

Unsteady and study double-diffusive convection utilizing different Prandtl number fluids in different type of geometries in the presence of uniform and non-uniform boundary conditions have been studied in [22–29]. Ren and Wan [30] studied the heat and mass transfer simultaneously in laminar moist air inside a vertical channel. Wang et al. [31] has investigated unsteady double-diffusive convection in the presence of Soret and Dufour effects in a horizontal cavity and discussed the impact of buoyancy ratio on flow, heat, and mass transfer.

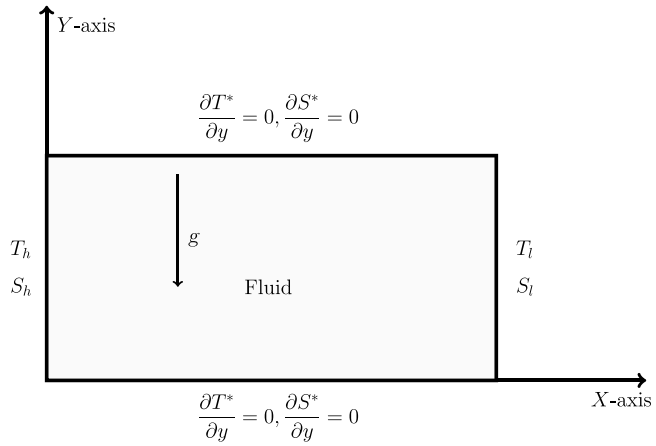

Fig. 1. Geometry of the considered problem.

Numerical investigation of buoyancy effect on thermosolutal convection in a horizontal annular porous cavity has been performed by Ja and Cheddadi [32]. Sheremet [33] numerically analyzed the influence of thermal diffusion (Soret) and diffusive thermal (Dufour) effects on nonstationary regimes of conjugate convective heat and mass transfer in an enclosure in the presence of heat conductive walls of finite thickness. Results obtained refer to investigating processes in chemical reactors, in growth of bulk single crystals, and in material working, e.g., during melting. Groşan et al. [34] numerically investigated the effect of thermophoresis on double diffusive natural convection in a differentially heated square cavity having a wavy wall filled with a Newtonian fluid containing suspended aerosol particles. Streamlines, isotherms, isoconcentration contours, average Nusselt number, and fluid flow rate are presented and discussed in detail. Kuznetsov and Sheremet [35,36] have investigated double diffusive natural convection in two and three dimensional geometries respectively. The results showed that the flow structure, heat, and mass transfer phenomenas are significantly influences by the Rayleigh number, Lewis number, buoyancy ratio and other parameters.

In literature, due to increasing mathematical complexities with a comparison to purely thermal diffusion problem, most of the study is limited to buoyancy imposed by temperature gradients only, thereby neglecting an interaction of the flow field with the solute gradients. This interaction with appropriate solute boundary conditions is considered in the present work. From a very recent study of [37] for thermohaline stratification modeling in mine water for geothermal energy recovery from flooded mines, one can understand the applicability of double-diffusion processes. In their study, authors claimed that no scientific explanation is available for the layering phenomenon of both temperature and salinity in large bodies of subterranean water (e.g., mine water). An experimental study of this kind is a quite cumbersome task. Besides, from earlier numerical studies, it is hard to understand the flow behavior of double-diffusion processes completely. Therefore, conclusions from a few cases are not transposable to another case. The demands for additional information and a better understanding of this phenomenon have also increased.

Heat transfer utilizing very low, low, and moderate Prandtl number fluids and combined heat and mass transfer convection utilizing mostly moderate Prandtl number fluids in the different types of cavities have been investigated widely in the literature survey of the present study. But only limited studies have been done for the combined heat and mass transfer convection utilizing low Prandtl number fluids. In all the literature articles, to visualize the fluid flow, authors have used streamline techniques, whereas heat and mass transfer variation in enclosures have been discussed by the isotherms and isoconcentrations contours. But those are not enough to do the tasks because they

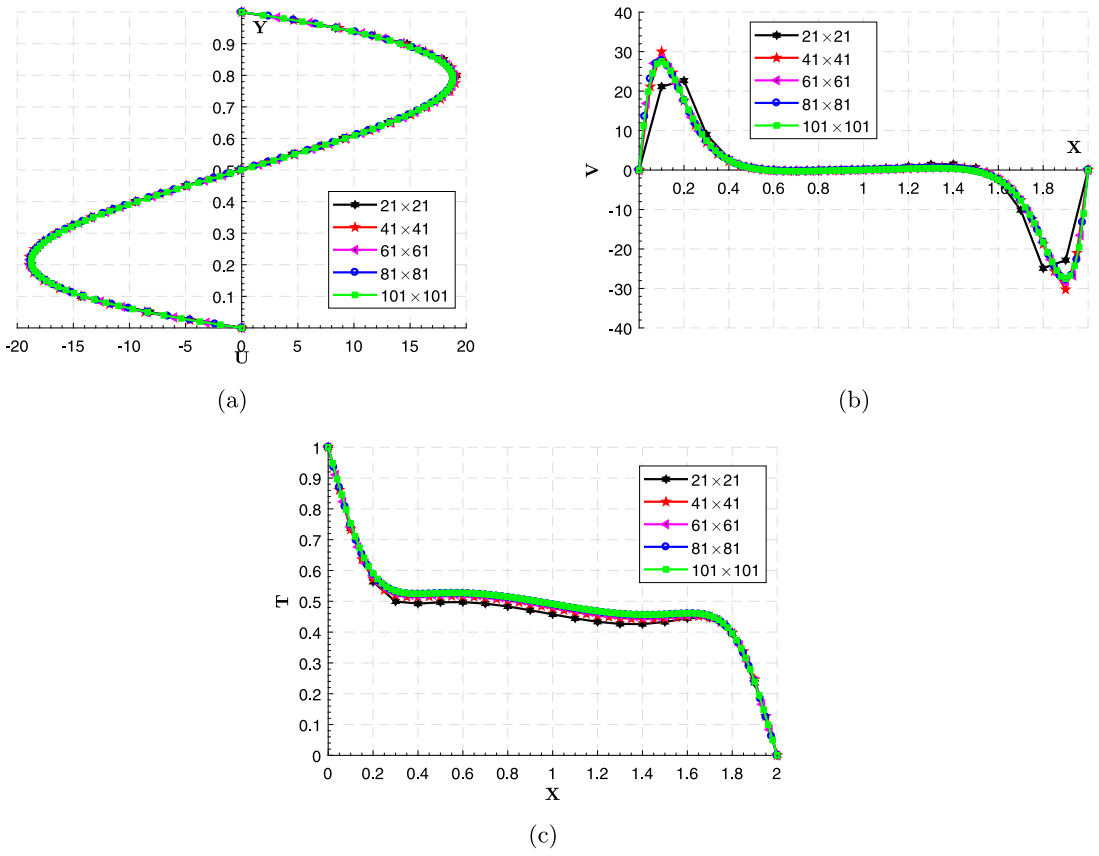

Fig. 2. Grid independent test for (a) U-velocity, (b) V-velocity, and (c) Temperature (T) along the mid of the enclosure.

indicate the temperature and concentration along the lines joining the points which have equal temperature and concentration respectively and fails to induce the energy and mass distribution in the enclosures in the context of magnitude and direction like streamlines. So we need something similar to the streamlines for better visualization of heat and mass transfers in the enclosures. For better visualization of heat transport in enclosures filled with fluids, the first time the heatline technique introduced by Kimura and Bejan [38], which gives better insight over isotherms approach. Later on, this visualization technique was adopted and extended for heat and mass transfer by Costa [39] and introduced mass function and massline analogy to visualize mass transfer in the fluid flow, which gives comparatively better insight to mass transport characteristics of fluid flow than isoconcentrations (isosolutes) approach. The limited use of heat and mass lines techniques are noticed in the literature so far. We are listing some research articles in which authors have used these techniques.

Rahman et al. [40] numerically investigated unsteady heat and mass transport with heatline and massline inside a ventilated cavity. Hussain [41] considered an inclined square cavity with non-uniform heating and salting to study the double-diffusive natural convection in the presence of an inclined magnetic field with heatlines and entropy generation. Alsabery et al. [42] studied the conjugate natural convection in a square cavity filled with a nanofluid with sinusoidal temperature variations on both horizontal walls is visualized by heatlines. Hu et al. [43] numerically investigated the natural convection heat and moisture transfer simultaneously in an inclined building enclosure filled with moist air. Heatline visualization of natural convection in a thick walled open cavity filled with a nanofluid has been investigated by Bondareva et al. [44]. Results showed that heatlines visualization technique is quite useful to study the transport of heat transfer inside the enclosure in addition to the isotherms. In these studies authors have been discussed the heatlines and masslines in addition to the isotherms and isosolutes for better understating of heat and mass transport phenomena inside the enclosures.

In order to increase the perception and understanding of this kind of processes where thermal and solute gradients develop due to natural convection phenomenon utilizing low and moderate Prandtl number fluids using heat and mass lines techniques, a typical study is considered and well documented the various conditions of technical processes by varying the considered parameters. To the author's best knowledge, thermo-solute natural convection with heat and mass lines in a uniformly heated and soluted rectangular enclosure for low Prandtl number fluids has not reported yet in the literature. To analyze the flow, heat and mass transfers for low Prandtl number, results are presented in terms of streamlines, isotherms, isosolutes, heatlines and masslines for the various parameters like: Rayleigh number (Ra), Prandtl number (Pr), Lewis number (Le), and Buoyancy ratio (N).

2. Mathematical formulation

2.1. Physical description

The geometrical description of the present problem, along with the thermal and solute boundary conditions, is shown in Fig. 1. The laminar unsteady incompressible flow is considered in a rectangular enclosure. We are considered the low and moderate Prandtl number fluids in the enclosure. The aspect ratio of the enclosure is assumed to be 2. The left wall maintains higher temperature (T_h) and solute (S_h) while the right wall is kept at lower temperature (T_l) and solute (S_l) such that $T_h > T_l$ and $S_h > S_l$. No-slip velocity boundary condition is applied to the boundaries of the enclosure. The horizontal walls are adiabatic and non-diffusive. The thermosolute natural convection effect is modeled

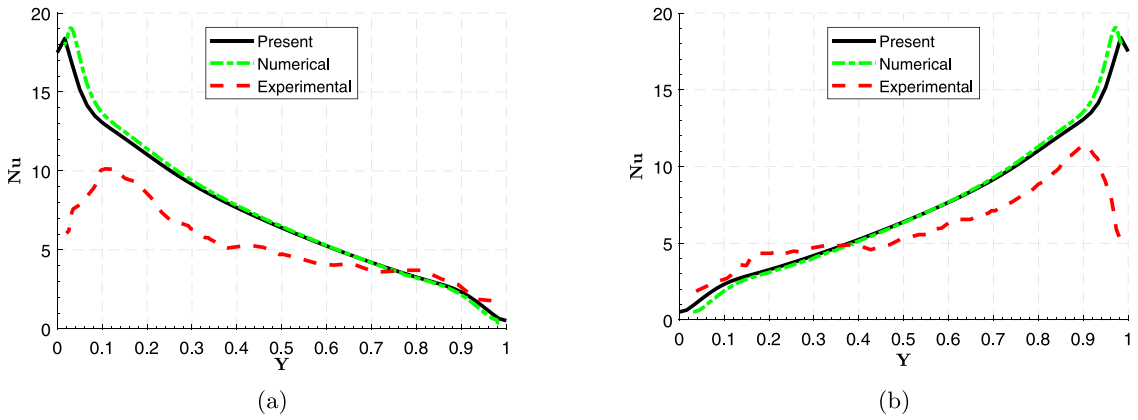

Fig. 3. Comparison of local Nusselt number along the (a) hot wall and (b) cold wall with Kishor et al. [45].

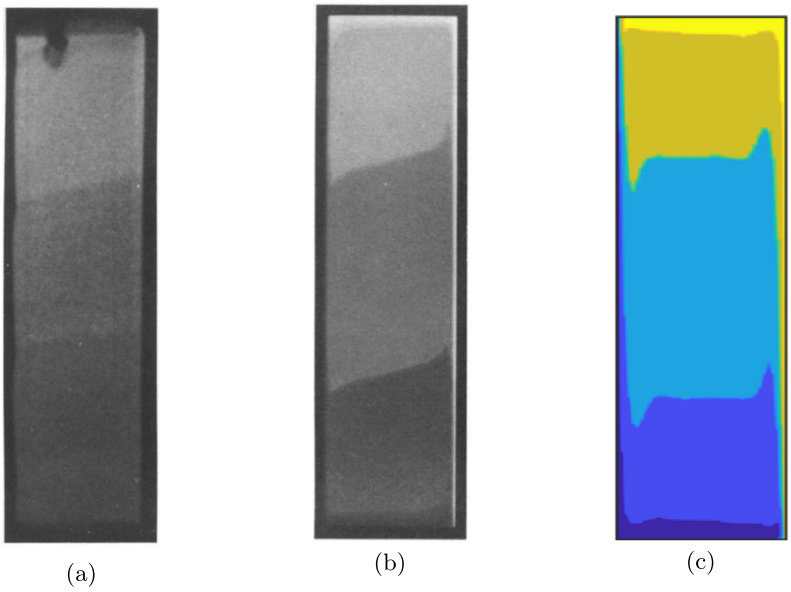

Fig. 4. Comparison of concentration distribution in the enclosure (a) experimental, (b) numerical of Han and Kuehn [46], and (c) present study.

by using Boussinesq approximation. Effect of Joule heating, thermal radiation, chemical reaction, and viscous dissipation are assumed to be neglected. Furthermore, the cross-diffusion effects are assumed to be neglected.

2.2. Governing equations

The two-dimensional, unsteady, laminar, and incompressible fluid is considered in the domain of the problem. The effect of density on temperature and solute is considered only in the body force term. The dimensional and non-dimensional governing equations with boundary conditions are presented below.

2.2.1. Governing equations in the dimensional form

The dimensional form of the governing equations are the continuity, the x- and y-components of the Navier–Stokes equations, the energy equation, and the solute equation as given below:

$$\frac{\partial u}{\partial x}+\frac{\partial v}{\partial y}=0, \tag{1}$$

$$\rho\left(\frac{\partial u}{\partial t}+u\frac{\partial u}{\partial x}+v\frac{\partial u}{\partial y}\right)=-\frac{\partial p}{\partial x}+\mu\left(\frac{\partial^2 u}{\partial x^2}+\frac{\partial^2 u}{\partial y^2}\right), \tag{2}$$

$$\rho\left(\frac{\partial v}{\partial t}+u\frac{\partial v}{\partial x}+v\frac{\partial v}{\partial y}\right)=-\frac{\partial p}{\partial y}+\mu\left(\frac{\partial^2 v}{\partial x^2}+\frac{\partial^2 v}{\partial y^2}\right)+\rho\left[\beta_{T^*}\left(T^*-T_l^*\right)+\beta_{S^*}\left(S^*-S_l^*\right)\right]g, \tag{3}$$

$$\rho c_p\left(\frac{\partial T^*}{\partial t}+u\frac{\partial T^*}{\partial x}+v\frac{\partial T^*}{\partial y}\right)=k\left(\frac{\partial^2 T^*}{\partial x^2}+\frac{\partial^2 T^*}{\partial y^2}\right), \tag{4}$$

$$\frac{\partial S^*}{\partial t}+u\frac{\partial S^*}{\partial x}+v\frac{\partial S^*}{\partial y}=D\left(\frac{\partial^2 S^*}{\partial x^2}+\frac{\partial^2 S^*}{\partial y^2}\right). \tag{5}$$

2.2.2. Initial and boundary conditions in dimensional form

The initial and boundary conditions in dimensional form for the governing Eqs. (1)–(5) are as follows:

$$\text{at}\quad t=0: u(x,y,0)=v(x,y,0)=T^*(x,y,0)=S^*(x,y,0)=0 \tag{6}$$

$$\left.\begin{aligned}&\text{at}\quad t>0,\\&u=v=0,\ \frac{\partial T^*}{\partial y}=\frac{\partial S^*}{\partial y}=0,\ \text{along the bottom wall},\\&u=v=0,\ T^*=S^*=0,\ \text{along the right wall},\\&u=v=0,\ \frac{\partial T^*}{\partial y}=\frac{\partial S^*}{\partial y}=0,\ \text{along the top wall}\\&u=v=0,\ T^*=S^*=1,\ \text{along the left wall},\end{aligned}\right\} \tag{7}$$

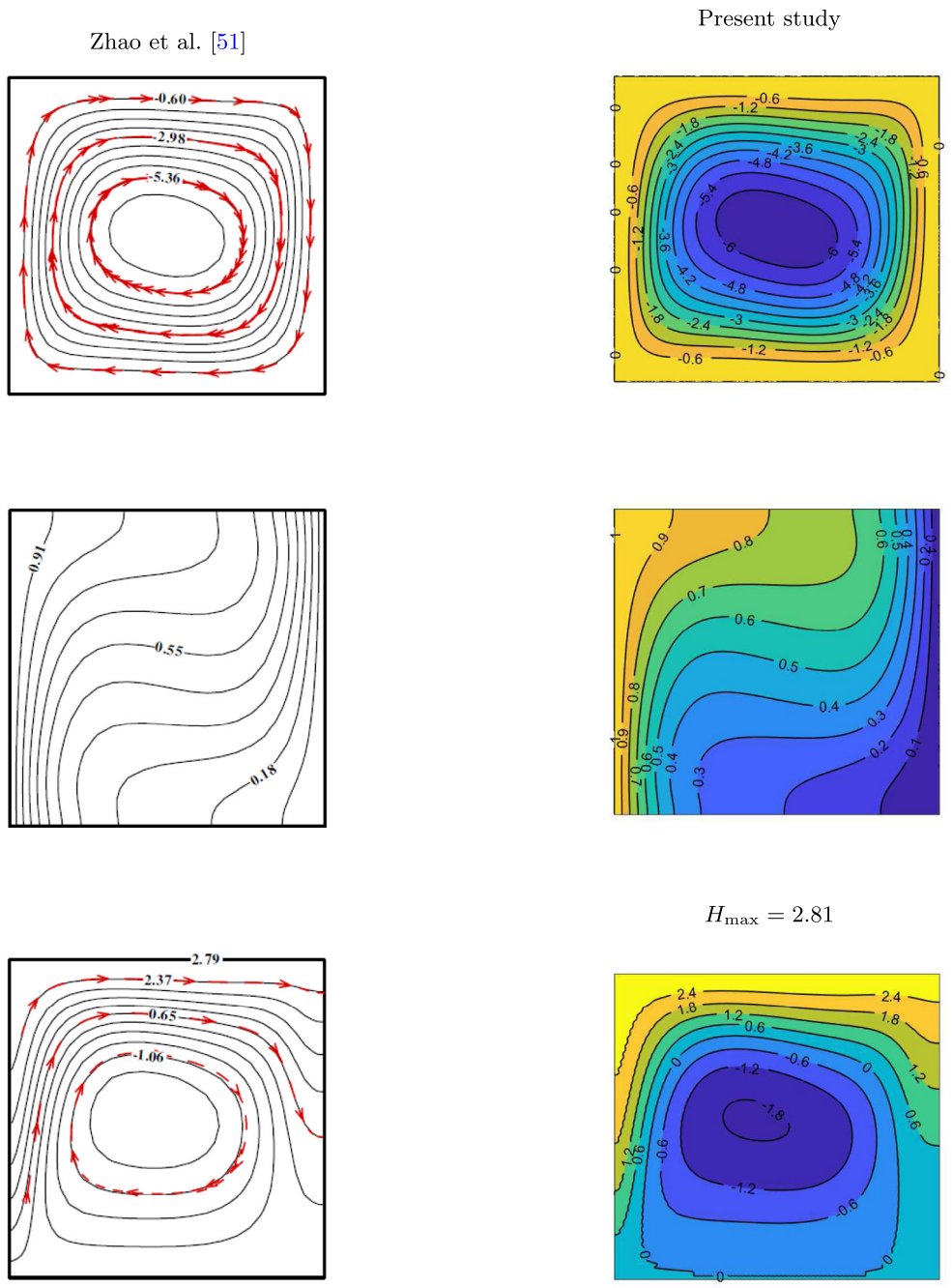

Fig. 5. Comparison of streamlines (top row), isotherms (middle row), and heatlines (bottom row) for Ra = 10^4 and Pr = 0.71 with Zhao et al. [47].

2.2.3. Non-dimensional governing equations

The non-dimensional form of Eqs. (1)–(5) in stream function, vorticity, temperature, and solute are obtained by defining $u = \frac{\partial \psi}{\partial y}$ and $v = -\frac{\partial \psi}{\partial x}$ and the vorticity $\omega = \frac{\partial v}{\partial x} - \frac{\partial u}{\partial y}$ and using the following non-dimensional parameters

$$X = \frac{x}{L}, \quad Y = \frac{y}{L}, \quad U = \frac{uL}{\alpha}, \quad V = \frac{vL}{\alpha}, \quad \tau = \frac{t\alpha}{L^2}, \quad \Psi = \frac{\psi}{\alpha},$$
$$P = \frac{pL^2}{\rho\alpha^2}, \quad \mathrm{Pr} = \frac{\nu}{\alpha}, \quad \mathrm{Le} = \frac{\alpha}{D}, \quad \Omega = \frac{\omega L^2}{\alpha}, \quad T = \frac{T^* - T_l^*}{T_h^* - T_l^*} \tag{8}$$
$$S = \frac{S^* - S_l^*}{S_h^* - S_l^*}, \quad \mathrm{Ra} = \frac{g\beta_{T^*}\left(T_h^* - T_l^*\right)L^3\,\mathrm{Pr}}{\nu^2}, \quad \mathrm{N} = \frac{\beta_{S^*}\left(S_h^* - S_l^*\right)}{\beta_{T^*}\left(T_h^* - T_l^*\right)},$$

is as follows:

$$\frac{\partial^2 \Psi}{\partial X^2} + \frac{\partial^2 \Psi}{\partial Y^2} = -\Omega \tag{9}$$
$$\frac{\partial \Omega}{\partial \tau} + U\frac{\partial \Omega}{\partial X} + V\frac{\partial \Omega}{\partial Y} = \mathrm{Pr}\left(\frac{\partial^2 \Omega}{\partial X^2} + \frac{\partial^2 \Omega}{\partial Y^2}\right) + \mathrm{Ra}\,\mathrm{Pr}\left(\frac{\partial T}{\partial X} + \mathrm{N}\frac{\partial S}{\partial X}\right) \tag{10}$$
$$\frac{\partial T}{\partial \tau} + U\frac{\partial T}{\partial X} + V\frac{\partial T}{\partial Y} = \frac{\partial^2 T}{\partial X^2} + \frac{\partial^2 T}{\partial Y^2}, \tag{11}$$
$$\frac{\partial S}{\partial \tau} + U\frac{\partial S}{\partial X} + V\frac{\partial S}{\partial Y} = \frac{1}{\mathrm{Le}}\left(\frac{\partial^2 S}{\partial X^2} + \frac{\partial^2 S}{\partial Y^2}\right). \tag{12}$$

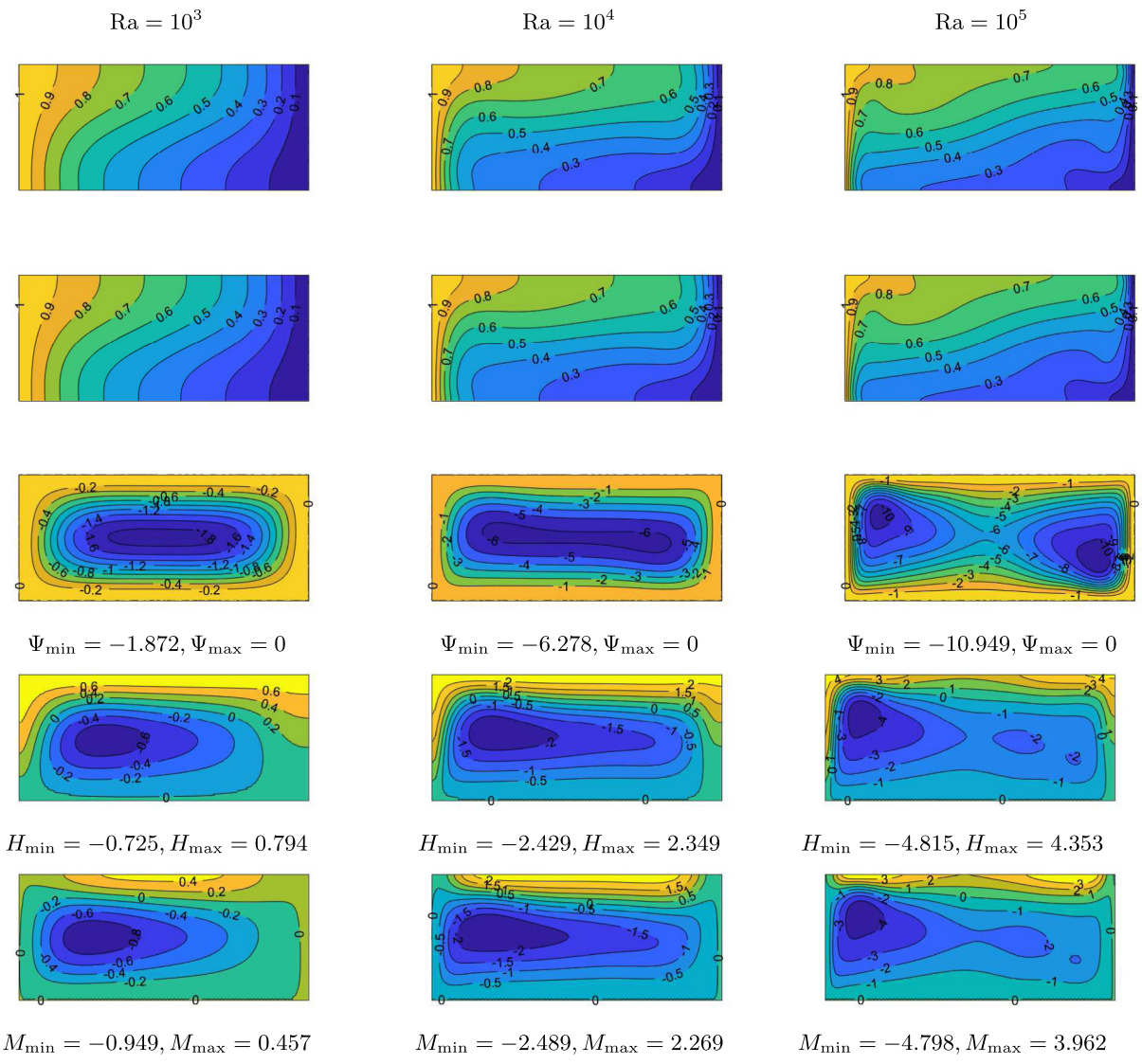

Fig. 6. Isotherms (top row), isosolutes (2rd row), streamlines (3rd row), heatlines (4th row), and masslines (bottom row) for different Rayleigh numbers at Pr = 0.71, Le = 1, and N = 1.

2.2.4. Non-dimensional initial and boundary conditions

The non-dimensional form of initial and boundary conditions [48, 49] for the non-dimensional flow governing Eqs. (9)–(12) are as follows:

$$\text{at} \quad \tau = 0 : \Psi(X,Y,0) = \Omega(X,Y,0) = T(X,Y,0) = S(X,Y,0) = 0 \tag{13}$$

$$\left.\begin{aligned} &\text{at} \quad \tau > 0, \\ &\Psi = 0, \Omega = -\frac{\partial^2 \Psi}{\partial Y^2}, \frac{\partial T}{\partial Y} = \frac{\partial S}{\partial Y} = 0, \ \text{along the bottom wall}, \\ &\Psi = 0, \Omega = -\frac{\partial^2 \Psi}{\partial X^2}, T = S = 0, \ \text{along the right wall}, \\ &\Psi = 0, \Omega = -\frac{\partial^2 \Psi}{\partial Y^2}, \frac{\partial T}{\partial Y} = \frac{\partial S}{\partial Y} = 0, \text{along the top wall}, \\ &\Psi = 0, \Omega = -\frac{\partial^2 \Psi}{\partial X^2}, T = S = 1, \ \text{along the left wall}, \end{aligned}\right\} \tag{14}$$

We consider the no-slip velocity boundary conditions, i.e. $U = V = 0$ along all the walls of the cavity.

The stream function is obtained from the definition

$$U = \frac{\partial \Psi}{\partial Y} \quad \text{and} \quad V = -\frac{\partial \Psi}{\partial X} \tag{15}$$

Which yields a single equation:

$$\frac{\partial^2 \Psi}{\partial X^2} + \frac{\partial^2 \Psi}{\partial Y^2} = \frac{\partial U}{\partial Y} - \frac{\partial V}{\partial X}. \tag{16}$$

The minus sign of Ψ indicates that the direction of flow is clockwise while the plus sign of Ψ denotes the direction of flow is anti-clockwise in the enclosure. It is taken that $\Psi = 0$ at the solid boundaries.

We denoted the local heat transfer coefficient along the left vertical wall as the local Nusselt number (Nu) and is defined by

$$\text{Nu} = -\frac{\partial T}{\partial X}. \tag{17}$$

The total heat transfer from the left vertical wall is denoted by the average Nusselt number (Nu_{avg}) and is defined as

$$\text{Nu}_{\text{avg}} = \int_0^1 \text{Nu} \, dY. \tag{18}$$

The local mass transfer coefficient along the left vertical wall is denoted by the local Sherwood number (Sh) and is given by

$$\text{Sh} = -\frac{\partial S}{\partial X}. \tag{19}$$

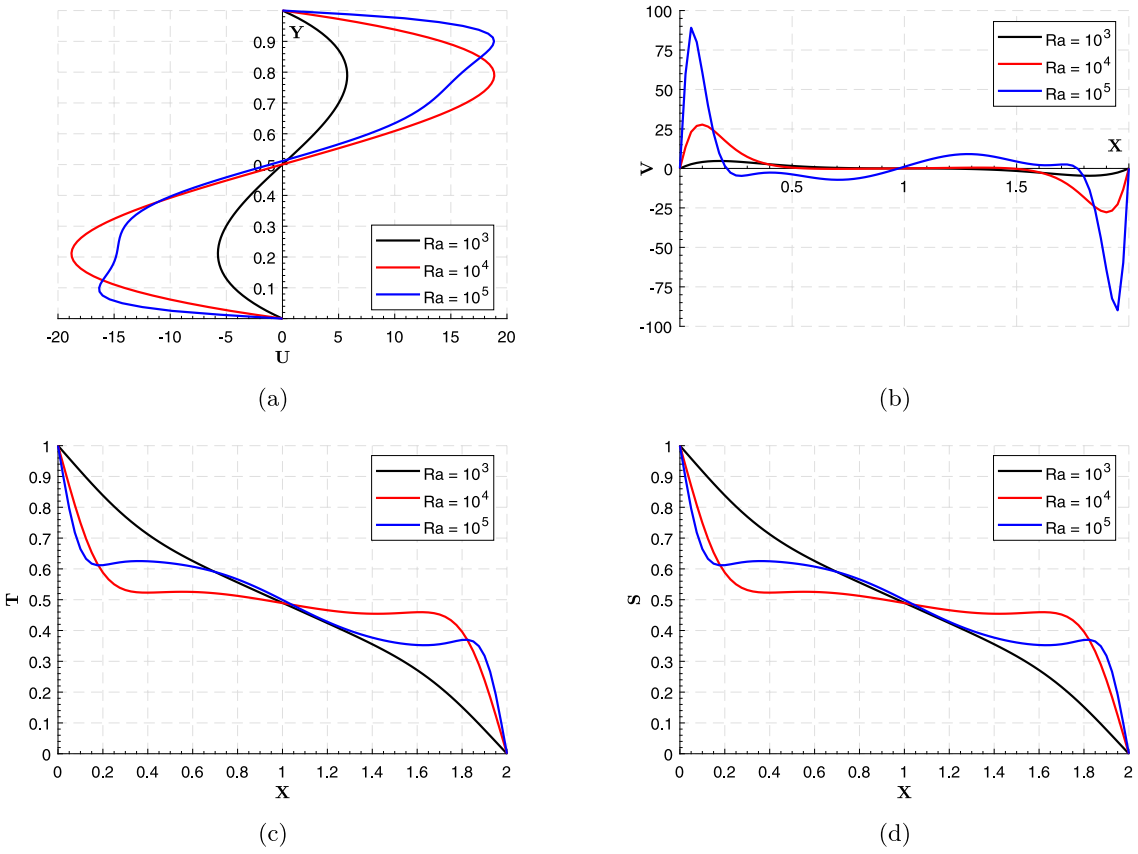

Fig. 7. Variation of (a) horizontal velocity, (b) vertical velocity, (c) temperature (T), and (d) solute (S) along the horizontal mid of cavity for different Rayleigh numbers at Pr = 0.71, Le = 1, and N = 1.

The total mass transfer from the left vertical wall is denoted by the average Sherwood number $(\mathrm{Sh}_{\mathrm{avg}})$ and is defined by

$$\mathrm{Sh}_{\mathrm{avg}} = \int_0^1 \mathrm{Sh}\, \mathrm{d}Y. \tag{20}$$

2.3. Heat function

Heat function [38,39] in the dimensional form is denoted as h and defined as

$$-\frac{\partial h}{\partial x} = \rho c_p v \left(T^* - T_l^*\right) - k\frac{\partial T^*}{\partial y} \tag{21}$$

$$\frac{\partial h}{\partial y} = \rho c_p u \left(T^* - T_l^*\right) - k\frac{\partial T^*}{\partial x} \tag{22}$$

We express Eqs. (21) and (22) in the dimensionless form by employing the non-dimensional parameters defined in Eq. (8) as follows:

$$-\frac{\partial H}{\partial X} = VT - \frac{\partial T}{\partial Y} \tag{23}$$

$$\frac{\partial H}{\partial Y} = UT - \frac{\partial T}{\partial X} \tag{24}$$

where H is the dimensionless heat function and it is represented as

$$H = \frac{h}{k\left(T_h^* - T_l^*\right)} \tag{25}$$

The manipulation of Eqs. (23) and (24) yields the following partial differential equation for the heat function.

$$\frac{\partial^2 H}{\partial X^2} + \frac{\partial^2 H}{\partial Y^2} = \frac{\partial (UT)}{\partial Y} - \frac{\partial (VT)}{\partial X} \tag{26}$$

We can get the dimensionless heat function H in the inner region of the rectangular enclosure considered by solving either of Eq. (23) or Eq. (24) or Eq. (26). The drawing of isolines of the heat function provides heatlines.

The initial condition in non-dimensional form for the heat function H is $H(X, Y, \tau) = H_0(X, Y) = 0$.

The corresponding non-dimensional boundary condition for the heat function H are as follows:

$$\begin{aligned} &\text{for,} \quad X = 0 \text{ and } X = 2, \quad \frac{\partial H}{\partial X} = 0, \\ &\text{for,} \quad Y = 0, \quad H = 0, \\ &\text{for,} \quad Y = 1, \quad H = \mathrm{Nu}_{\mathrm{avg}}\,. \end{aligned} \tag{27}$$

2.4. Mass function

Mass function [39,50] in the dimensional form is denoted as m and defined as

$$-\frac{\partial m}{\partial x} = \rho v \left(S^* - S_l^*\right) - \rho D\frac{\partial S^*}{\partial y} \tag{28}$$

$$\frac{\partial m}{\partial y} = \rho u \left(S^* - S_l^*\right) - \rho D\frac{\partial S^*}{\partial x} \tag{29}$$

We express Eqs. (28) and (29) in the dimensionless form by employing the non-dimensional parameters defined in Eq. (8) as follows:

$$-\frac{\partial M}{\partial X} = VS - \frac{1}{\mathrm{Le}}\frac{\partial S}{\partial Y} \tag{30}$$

$$\frac{\partial M}{\partial Y} = US - \frac{1}{\mathrm{Le}}\frac{\partial S}{\partial X} \tag{31}$$

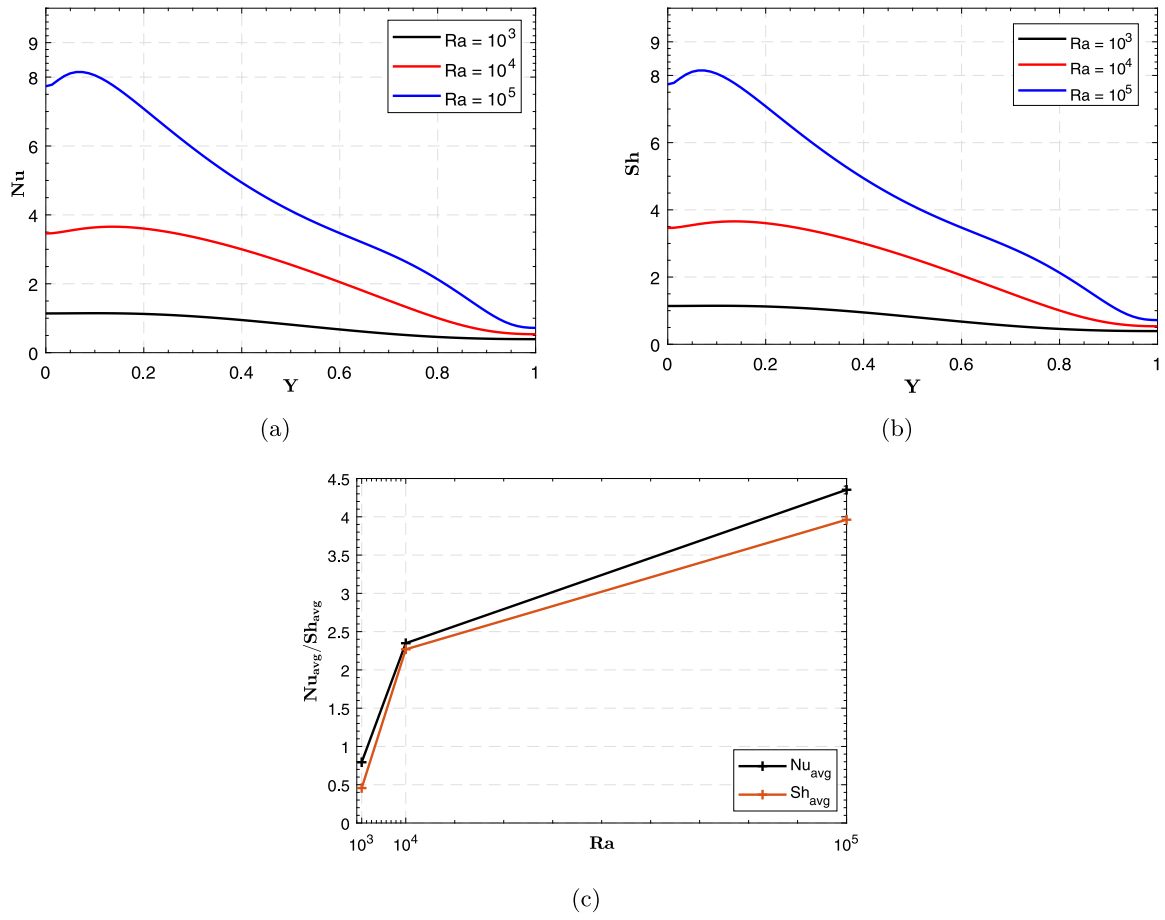

Fig. 8. Comparison of (a) Local Nusselt number, (b) Local Sherwood number, and (c) Average Nusselt and Sherwood number for different Rayleigh numbers at Pr = 0.71, Le = 1, and N = 1.

Table 1
Comparison of average Nusselt number along hot and cold walls with Kishor et al. [45].

Ra	Wall	Experimental [45]	Numerical [45]	Present study
9.7×10^5	Hot	5.496	7.209	7.181
	Cold	5.962	7.209	7.181

Table 2
Comparison of average Nusselt number with previous works for different *Ra*-values.

	$Ra = 10^3$	$Ra = 10^4$	$Ra = 10^5$
Ref. [51]	1.118	2.243	4.519
Ref. [52]	1.108	2.201	4.43
Ref. [53]	1.118	2.245	4.522
Ref. [54]	1.087	2.195	4.45
Present study	1.32	2.80	4.35

where M is the non-dimensional mass function and it is defined as

$$M = \frac{m}{\mathrm{Le}\,\rho D\left(S_h^* - S_l^*\right)} \tag{32}$$

The manipulation of Eqs. (30) and (31) yields the following partial differential equation for the mass function.

$$\frac{\partial^2 M}{\partial X^2} + \frac{\partial^2 M}{\partial Y^2} = \frac{\partial (US)}{\partial Y} - \frac{\partial (VS)}{\partial X} \tag{33}$$

We can get the dimensionless mass function M in the inner region of the rectangular enclosure considered by solving either of Eq. (30) or Eq. (31) or Eq. (33). The drawing of isolines of the mass function provides masslines.

The initial condition in non-dimensional form for the mass function M is $M(X, Y, \tau) = M_0(X, Y) = 0$.

The corresponding non-dimensional boundary condition for the heat function M are as follows:

$$\begin{aligned} &\text{for,} \quad X = 0 \text{ and } X = 2, \quad \frac{\partial M}{\partial X} = 0, \\ &\text{for,} \quad Y = 0, \quad M = 0, \\ &\text{for,} \quad Y = 1, \quad M = \mathrm{Sh}_{\mathrm{avg}}\,. \end{aligned} \tag{34}$$

3. Solution procedure

The governing Eqs. (9)–(12) are discretized by the finite difference method. The diffusion term in the vorticity, energy, and solute equations is approximated by a second-order central difference scheme which gives a stable solution. Furthermore, a second order central differencing scheme is adopted for the convective terms. A second order accurate formula is used for the vorticity boundary condition, which is based on Woods [55]. The set of discretized governing equations are solved from the initial stage. Vorticity equation Eq. (10) is solved for a time step to compute the vorticity field in the computational domain. Then, the stream function equation Eq. (9) is solved by successive over-relaxation (SOR) method and once we have the stream function field, we obtain the velocity values. The value of relaxation parameter is assumed 1.3. At the same time step and using the new velocity values are used to solve the set of discretized equations for energy Eq. (11) and solute Eq. (12) transports in the computational domain. A computer code is written in the FORTRAN-95 to solve the algebraic equations obtained after the discretization process. Throughout the calculations, all the dependent variables are considered to be converged, if,

$$\left|\chi_{i,j}^{n+1} - \chi_{i,j}^{n}\right| \leq 10^{-7}, \tag{35}$$

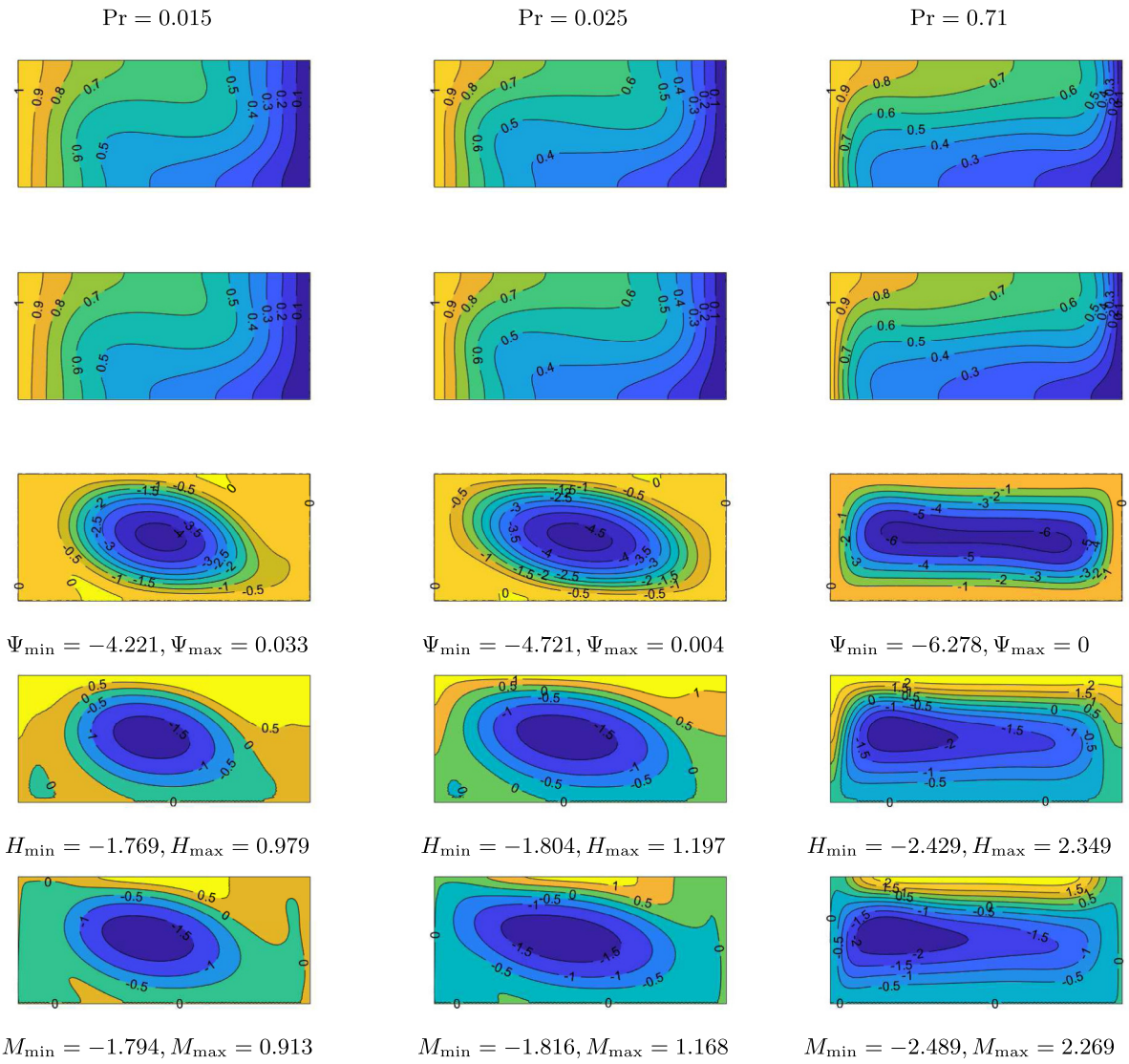

Fig. 9. Isotherms (top row), isosolutes (2rd row), streamlines (3rd row), heatlines (4th row), and masslines (bottom row) for different Prandtl numbers at Ra = 10^4, Le = 1, and N = 1.

where $\chi = (U, V, \Psi, \Omega, T, S)$, n is the iteration number and (i, j) denote the calculation node point.

4. Results and discussion

4.1. Grid independent test

The grid independent test has been performed and presented in Fig. 2 to make sure for the grid free solutions. We are considered five different grid systems: 21 × 21, 41 × 41, 61 × 61, 81 × 81, and 101 × 101 for Ra = 10^4, Pr = 0.71, Le = 1 and N = 1 for this purpose. There is no significant change is found after the grid size 81 × 81. Therefore all the results are obtained by using the grid 81 × 81 as an optimal grid size.

4.2. Experimental and numerical code validations

4.2.1. Experimental code validation

The numerical code developed to solve the flow governing equations in the present study has been validated with the experimental and numerical results of local Nusselt number along the hot and cold walls with Kishor et al. [45] presented in Fig. 3 and concentration distribution in the enclosure with Han and Kuehn [46] shown in Fig. 4. Table 1 shows the comparison of average Nusselt number along the hot and cold wall with the experimental and numerical values calculated in Kishor et al. [45]. For any given Rayleigh number, the observed difference may be attributed to the inherent experimental errors that include noise in the data, possible loss of fringes in the region very close to thermally active walls of the cavity (this factor also gets compounded due to the spatial resolution of the CCD camera employed in the experiments), etc. [45, p. 83]. So, in the light of authors above considerations, we may conclude that the numerical results of the present study have a satisfactory agreement with Kishor et al. [45], in fact, our numerical results are closer to experimental of Kishor et al. [45].

4.2.2. Numerical code validation

To validate the developed code in the present study, we compare streamlines, isotherms, and heatlines with Zhao et al. [47] presented in Fig. 5, and they show a good agreement. We are also compared the average Nusselt number for different Rayleigh numbers $\left(10^3 \le \mathrm{Ra} \le 10^5\right)$ of the present study with various benchmark research articles and given in Table 2. The average Nusselt number calculated in this study at 10^3 and 10^4 is better than the literature ones, and for 10^5, there is a

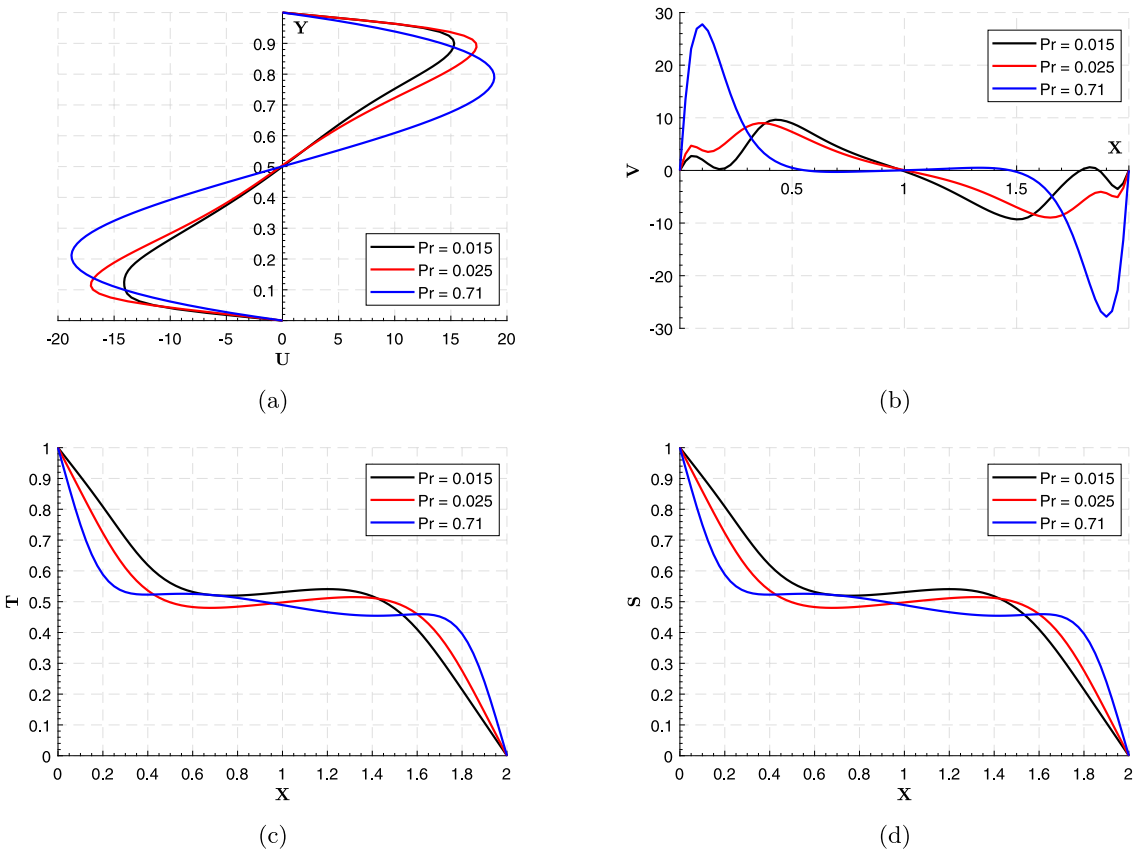

Fig. 10. Variation of (a) horizontal velocity, (b) vertical velocity, (c) temperature (T), and (d) solute (S) along the horizontal mid of cavity for different Prandtl numbers at $Ra = 10^4$, $Le = 1$, and $N = 1$.

deviation of ≈ 3%. Similar values of average Nusselt of this study is also noticed in Zhao et al. [47].

4.3. Interpretation of results for the rectangular cavity

The numerical simulations are performed for different parameters: Rayleigh number $(Ra = 10^3, 10^4, 10^5)$, Prandtl number $(Pr = 0.015, 0.025, 0.71)$, Lewis number $(Le = 1, 2, 5)$, and buoyancy ratio $(N = -1, 0, 1)$. The results, streamlines, isotherms, isosolute, heat and mass lines, horizontal and vertical mid velocities, temperature and solute along the horizontal mid of the enclosure, local and average Nusselt and Sherwood numbers are discussed for the above mentioned parameters.

4.3.1. Effect of Rayleigh number on fluid flow, thermal, and solute transfer

The ratio of the buoyancy forces to the viscous forces is defined as the Rayleigh number (Ra). The effects of buoyancy forces become stronger in comparison to the viscous force with the increment in the Rayleigh number, which significantly increases heat and solute transfers by convection due to the stronger buoyancy-driven flow with higher vertical velocity magnitude. Fig. 6 indicates the streamlines, isotherms, isosolutes, heatlines, and masslines for different Rayleigh numbers at $Pr = 0.71$, $Le = 1$, and $N = 1$. At $Ra = 10^3$, the isotherms are parallel to the sidewalls of the enclosure, which indicate that the conduction is dominated over the convection. The isotherms between left and right walls travel more distance to reach top wall from the bottom wall and become more curved when the Rayleigh number Ra augmented from 10^3 to 10^5, and this shows that the convection process significantly augmented.

Moreover, there is a significant increment in the temperature gradient on the left wall with the increment of the Rayleigh number. The isosolutes showed similar behavior when the Rayleigh number increases and solute gradient augmented significantly. This shows that the solute transfer enhanced considerably with the increase of Rayleigh number Ra from 10^3 to 10^5. These processes happen because, for low values of Rayleigh number, the buoyancy force is dominated by viscous force and causes the thermal and solutal boundary layer thicknesses thicker. With the rise in Rayleigh number, thermal and solute boundary layer thickness becomes thinner due to the domination of buoyancy force over viscous force. Consequently, strengthen in heat and solute transfer convection processes. At $Ra = 10^3$, the shape of streamlines are elliptical in the enclosure; it depicts that conduction is dominated. The shape of streamlines becomes non-elliptical with the increment of Rayleigh number and indicates that the fluid is rise from left and down from the right, which shows that the flow transfer becomes stronger; consequently, the convection process strengthens significantly. The same can be noted from the values of stream function for different Rayleigh numbers. The magnitude of Ψ_{min} enhances considerably with the increment in Rayleigh number yields progressively strengthens in the flow transfer and hence convection process.

Table 3
Comparison of horizontal and vertical velocities, temperature and solute along the vertical mid of the cavity for different Rayleigh numbers at $Pr = 0.71$, $Le = 1$, and $N = 1$.

	$Ra = 10^3$	$Ra = 10^4$	$Ra = 10^5$
U_{max}	5.77	18.87	18.85
U_{min}	−5.79	−18.80	−16.33
V_{max}	4.72	27.76	89.09
V_{min}	−5.65	−27.80	−89.86
T_{max}	0.66	0.74	0.72
T_{min}	0.35	0.27	0.28
S_{max}	0.66	0.74	0.72
S_{min}	0.35	0.27	0.28

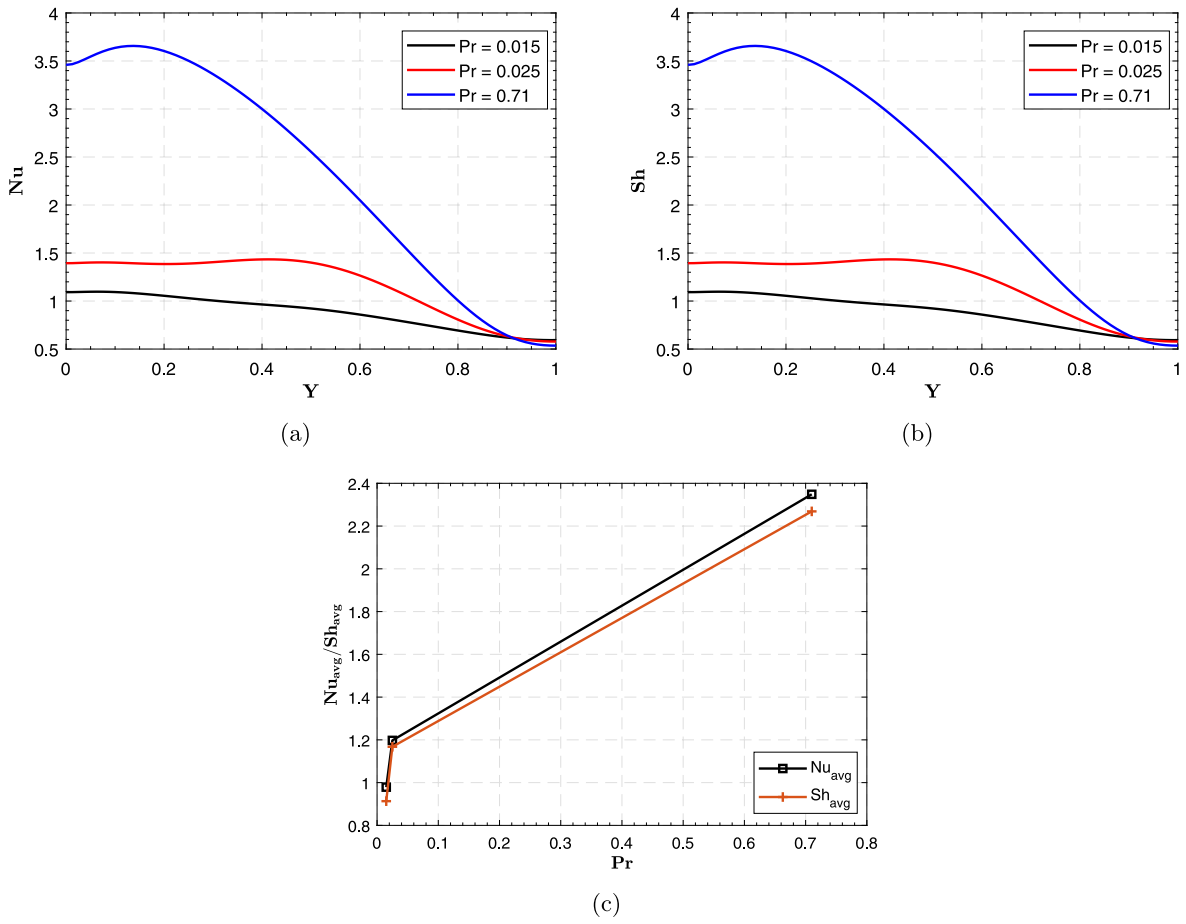

Fig. 11. Comparison of (a) Local Nusselt number, (b) Local Sherwood number, and (c) Average Nusselt and Sherwood number for different Prandtl numbers at Ra = 10^4, Le = 1, and N = 1.

Table 4
Comparison of average Nusselt and Sherwood numbers for different Rayleigh numbers at Pr = 0.71, Le = 1, and N = 1.

	Ra = 10^3	Ra = 10^4	Ra = 10^5
Nu_{avg}	0.794	2.349	4.353
Sh_{avg}	0.457	2.269	3.962

In the process of heat and solute transfer from higher temperature and solute wall to the low temperature and solute one, some heat and mass lines start to travel from the left wall and end on the right wall, and such heat and mass lines have positive values. These heat and mass lines are responsible for heat and solute transfer from left to the right wall, in other words, these can be turned as direct heat and solute transfer. And others have negative values and being generated inside the enclosure; these are responsible for the internal transfer of heat and solute, these may be called as thermal and solute mixing.

At Ra = 10^3, the H_{min} = −0.725 and M_{min} = −0.949 and H_{max} = 0.794 and M_{max} = 0.457, this indicates that the conduction is dominated over convection. As Rayleigh number is augmented from Ra = 10^3 to Ra = 10^5, the magnitude of both the positive and negative values is enhanced, and this depicts that the direct heat and mass transfer, as well as internal transfer, enhanced. Consequently, the convection rates due to heat and solute enhance significantly. We notice both positive and negative values significantly augmented with the increment in Rayleigh number. The internal heat transfer rate is dominated by the direct heat transfer rate for Ra = 10^3 because the magnitude of H_{min} is less than H_{max}. As Ra increases from 10^3 to 10^5 the magnitude of H_{min} and H_{max} both augmented significantly and the magnitude of H_{min} is greater than the H_{max}, this shows that the internal heat transfer rate dominates the direct heat transfer rate. Moreover, the magnitude of M_{min} and M_{max} both augmented significantly and the magnitude of M_{min} is greater than the M_{max}, from this we may conclude that the internal mass transfer rate dominates the direct mass transfer rate. Furthermore, it can be noticed that the magnitude of H_{min} is less than the magnitude of M_{min}; this indicates that the internal mass transfer rate dominates the internal heat transfer rate. However, the magnitude of H_{max} is greater than the magnitude of M_{max}; from this, we depict that the direct heat transfer rate dominates the direct mass transfer rate.

Fig. 7 illustrates the velocity components, temperature and solute distributions along the horizontal mid of cavity for different Rayleigh numbers at Pr = 0.71, Le = 1, and N = 1. For the smaller values of Rayleigh number, the horizontal and vertical velocities are low because of the domination of viscous force over the buoyancy force. When Rayleigh number increases the viscous force is strongly dominated by buoyancy force yields strengthens in the velocities. At Ra = 10^3, the distribution of temperature and solute along the horizontal mid of the cavity vary in almost linear manner; due to this, the heat and solute transfer occurs by pure conduction. The distribution of temperature and solute follows a nonlinear profile and enhancing the convention process with the increment in Rayleigh number. Fig. 8 depicts the local and average Nusselt and Sherwood numbers along the left wall of the enclosure for different Rayleigh numbers at Pr = 0.71, Le = 1, and N = 1. At Ra = 10^3, the local Nusselt and Sherwood numbers are almost equal to one; this indicates that the heat and mass transfer occurs due to the pure conduction process. As the Rayleigh number augmented, the buoyancy forces dominate the viscous ones. Table 3 presents the maximum and minimum values of horizontal and vertical velocities,

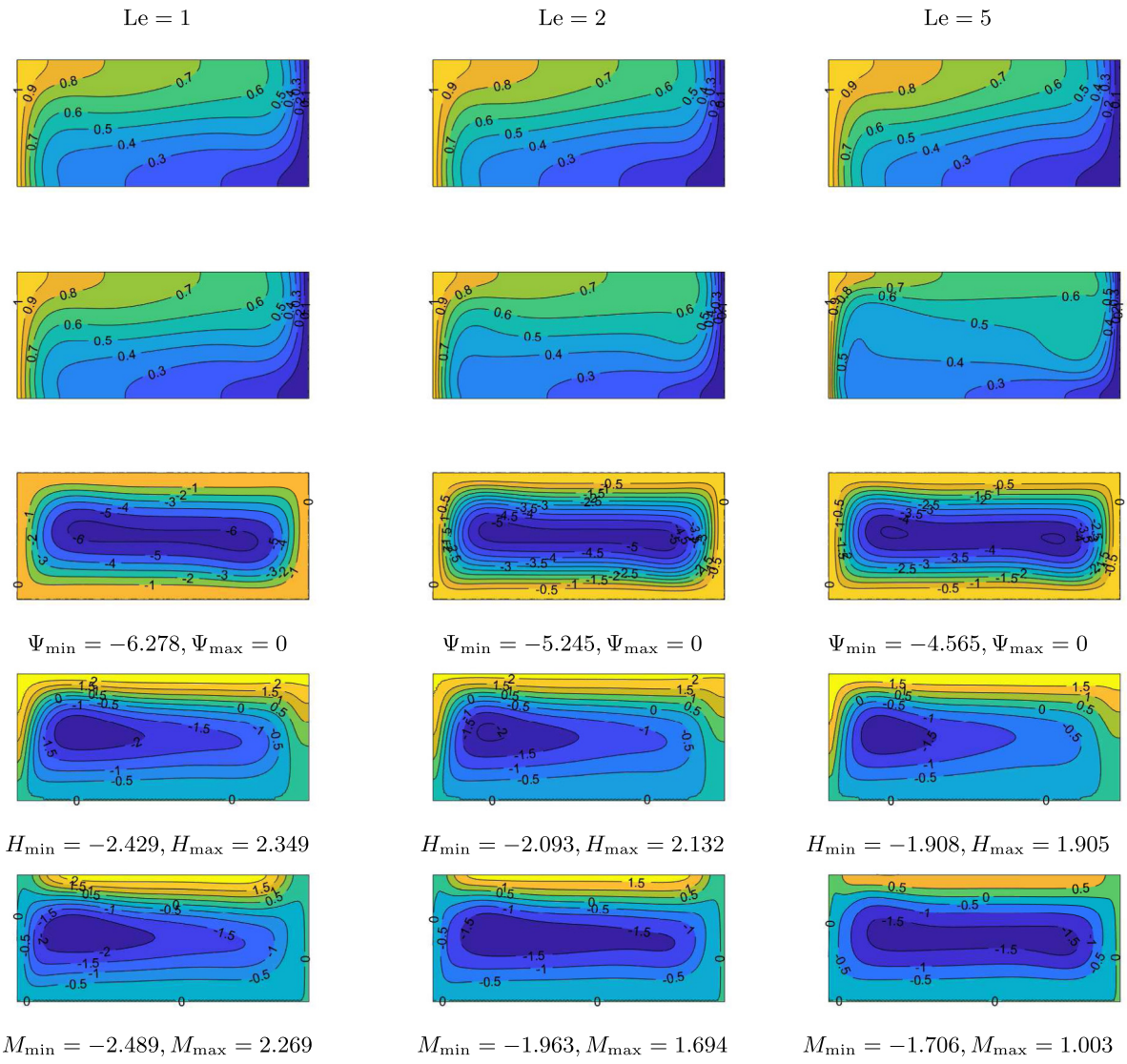

Fig. 12. Isotherms (top row), isosolutes (2rd row), streamlines (3rd row), heatlines (4th row), and masslines (bottom row) for different Lewis numbers at Ra = 10^4, Pr = 0.71, and N = 1.

temperature and solute along the vertical mid of the cavity for different Rayleigh numbers at Pr = 0.71, Le = 1, and N = 1. Fig. 8(c) and Table 4 illustrate that there is a significant enhancement in average Nusselt and Sherwood number with the increment in Rayleigh number whereas the average Nusselt number dominates the average Sherwood numbers, it means the total heat transfer dominates the total mass transfer.

4.3.2. Effect of Prandtl number on fluid flow, thermal, and solute transfer

The ratio of momentum diffusivity to the thermal diffusivity of the fluid is defined as the Prandtl number (Pr). In other words, we can say that the Prandtl number represents the ratios of the hydrodynamic boundary layer to the thermal boundary layer thicknesses. Fig. 9 Illustrates the streamlines, isotherms, isosolutes, heatlines, and masslines for different Prandtl numbers at Ra = 10^4, Le = 1, and N = 1. Most of the isotherms are parallel to the sidewalls of the enclosure, and it depicts that the pure conduction process is being happened. The isotherms between left and right walls, travel more distance to reach the top wall from the bottom wall and become more curved when Prandtl number Pr increases from 0.015 to 0.71, this indicates that the convection process significantly augmented. Moreover, there is a significant increment in the temperature gradient on the left wall with the increment of the Prandtl number. The isosolutes show almost similar patterns when the Prandtl number augmented and solute gradient increase significantly. This shows that the solute transfer enhanced considerably with the rise in Prandtl number Pr from 0.015 to 0.71. These effects may be noted because, for low values of Prandtl number, thermal diffusivity is dominated by momentum diffusivity. When Prandtl number rises the thermal diffusivity dominates the momentum diffusivity, this causes the enhancement in the heat and solute transfer, consequently, the convection process due to heat and solute. At Pr = 0.015, the circular type streamlines depict unicellular vortex with value, $\Psi_{min} = -4.221$ at the center of the enclosure but do not cover the whole enclosure, and it shows that conduction is dominated. The shape of streamlines becomes elliptical with the increase of Prandtl number and indicates that the fluid is rise from left and down from the right, which shows that the flow transfer rate is augmented significantly and at Pr = 0.71, the flow transfer rate is significantly high. The same may be noted from the values of stream function for different Prandtl number. The magnitude of Ψ_{min} enhances significantly with the increment in Prandtl number yields progressively strengthens in the flow convection process.

At Pr = 0.015, the heat and mass lines do not cover the whole enclosure, and the $H_{min} = -1.769$ and $M_{min} = -1.794$ and $H_{max} = 0.979$ and $M_{max} = 0.913$, this illustrates that the conduction is dominated over convection. As Prandtl number is augmented from Pr = 0.015 to Pr = 0.71, the heat and mass lines cover the whole enclosure,

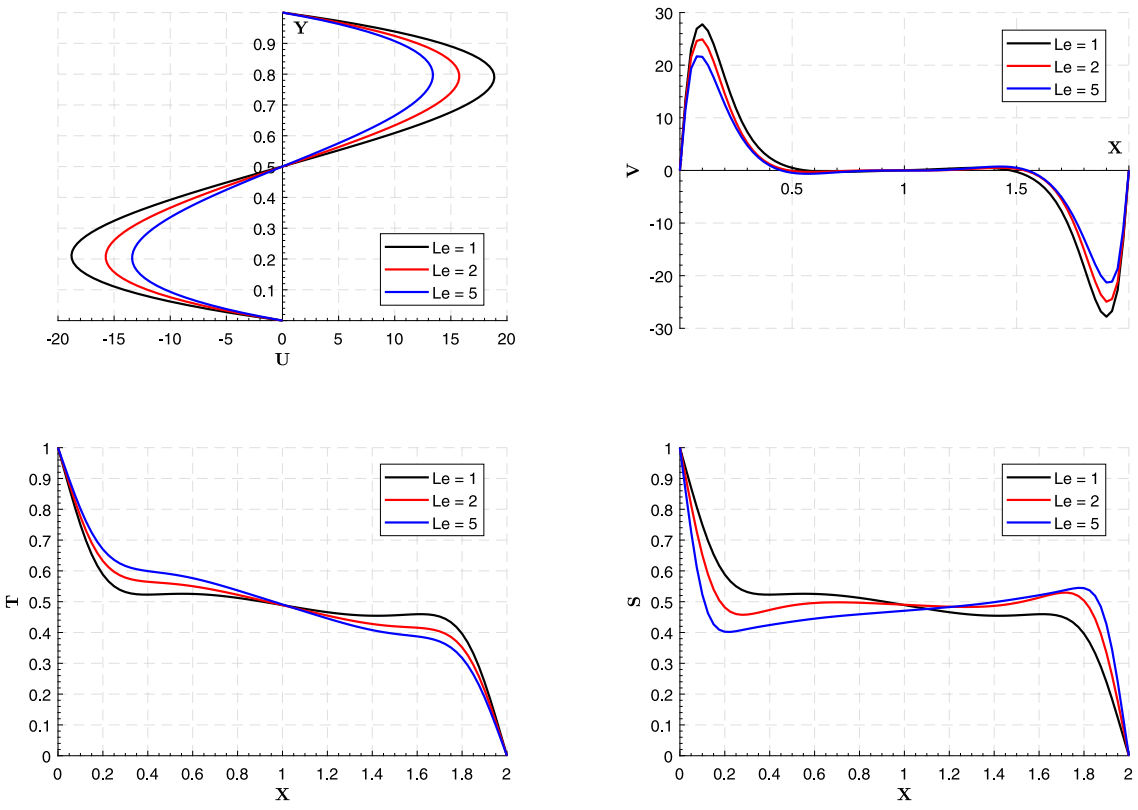

Fig. 13. Variation of velocity, temperature, solute, heat function, mass function, and stream function distributions in the mid of cavity for different Lewis numbers at Ra = 10^4, Pr = 0.71, and Le = 1.

the magnitude of both the positive and negative values are enhanced, and this indicates that the direct heat and mass transfer, as well as internal transfer, enhanced. Consequently, the convection rates due to heat and solute enhance significantly. We notice both positive and negative values significantly augmented with the increment in the Prandtl number. The magnitude of H_{min} and M_{min} is greater than the magnitude of H_{max} and M_{max}, this shows that the internal heat and mass transfer rates dominates the direct heat and mass transfer rates. Furthermore, it can be noticed that the magnitude of H_{min} is less than the magnitude of M_{min}; this indicates that the internal mass transfer rate dominates the internal heat transfer rate. However, the magnitude of H_{max} is greater than the magnitude of M_{max}, from this we can notice that the direct heat transfer rate dominates the direct mass transfer rate.

Fig. 10 depicts the velocity components, temperature and solute distributions along the horizontal mid of cavity for different Prandtl numbers at Ra = 10^4, Le = 1, and N = 1. For the smaller values of Prandtl number, the horizontal and vertical velocities are low because of the domination of momentum diffusivity over the thermal diffusivity. When Prandtl number increases, the momentum diffusivity is strongly dominated by thermal diffusivity yields strengthens in the velocities. With the rise in Prandtl number, there is significant fall in temperature and solute along with the horizontal mid of the cavity, this cause enhancement in convention process due to heat and solute. Fig. 11 illustrates the local and average Nusselt and Sherwood numbers along the left wall of the enclosure for different Prandtl numbers at Ra = 10^4, Le = 1, and N = 1.

At Pr = 0.015, the local Nusselt and Sherwood numbers are almost equal to one, and this indicates that the heat transfer occurs due to the pure conduction process. Table 5 shows the maximum and minimum values of horizontal and vertical velocities, temperature and solute along with the vertical mid of the cavity for different Prandtl numbers at Ra = 10^4, Le = 1, and N = 1. Fig. 11(c) and Table 6 show that there is a significant enhancement in average Nusselt and Sherwood number with the increment in Prandtl number, however, the total heat transfer rate dominates the overall mass transfer rate.

Table 5
Comparison of horizontal and vertical velocities, temperature and solute along the vertical mid of the cavity for different Prandtl numbers at Ra = 10^4, Le = 1, and N = 1.

	Pr = 0.015	Pr = 0.025	Pr = 0.71
U_{max}	15.30	17.29	18.87
U_{min}	−14.11	−17.07	−18.80
V_{max}	9.63	8.99	27.76
V_{min}	−9.30	−8.96	−27.80
T_{max}	0.67	0.67	0.74
T_{min}	0.39	0.35	0.27
S_{max}	0.67	0.67	0.74
S_{min}	0.39	0.35	0.27

Table 6
Comparison of average Nusselt and Sherwood numbers for different Prandtl numbers at Ra = 10^4, Le = 1, and N = 1.

	Pr = 0.015	Pr = 0.025	Pr = 0.71
Nu_{avg}	0.979	1.197	2.349
Sh_{avg}	0.913	1.168	2.269

4.3.3. *Effect of Lewis number on fluid flow, thermal, and solute transfer*

The Lewis number (Le) is a dimensionless number defined as the ratio of thermal diffusivity to mass diffusivity. It is used to characterize fluid flows where simultaneous heat and mass transfer occur. Fig. 12 presents the isotherms, isosolutes, streamlines, heatlines, and masslines for different Lewis numbers at Ra = 10^4, Pr = 0.71, and N = 1. There is no significant effect of Lewis numbers on isotherms, but the temperature gradient decreases as Lewis number augmented, this indicates that the convection rate is dominated by conduction rate. When the Lewis number Le increases from 1 to 5, the shapes of isosolutes change and the solute gradient increases slightly on the left wall, it shows that the convection rate is high at Le = 1 however, convection rate is dominated by conduction with the increment in Lewis number.

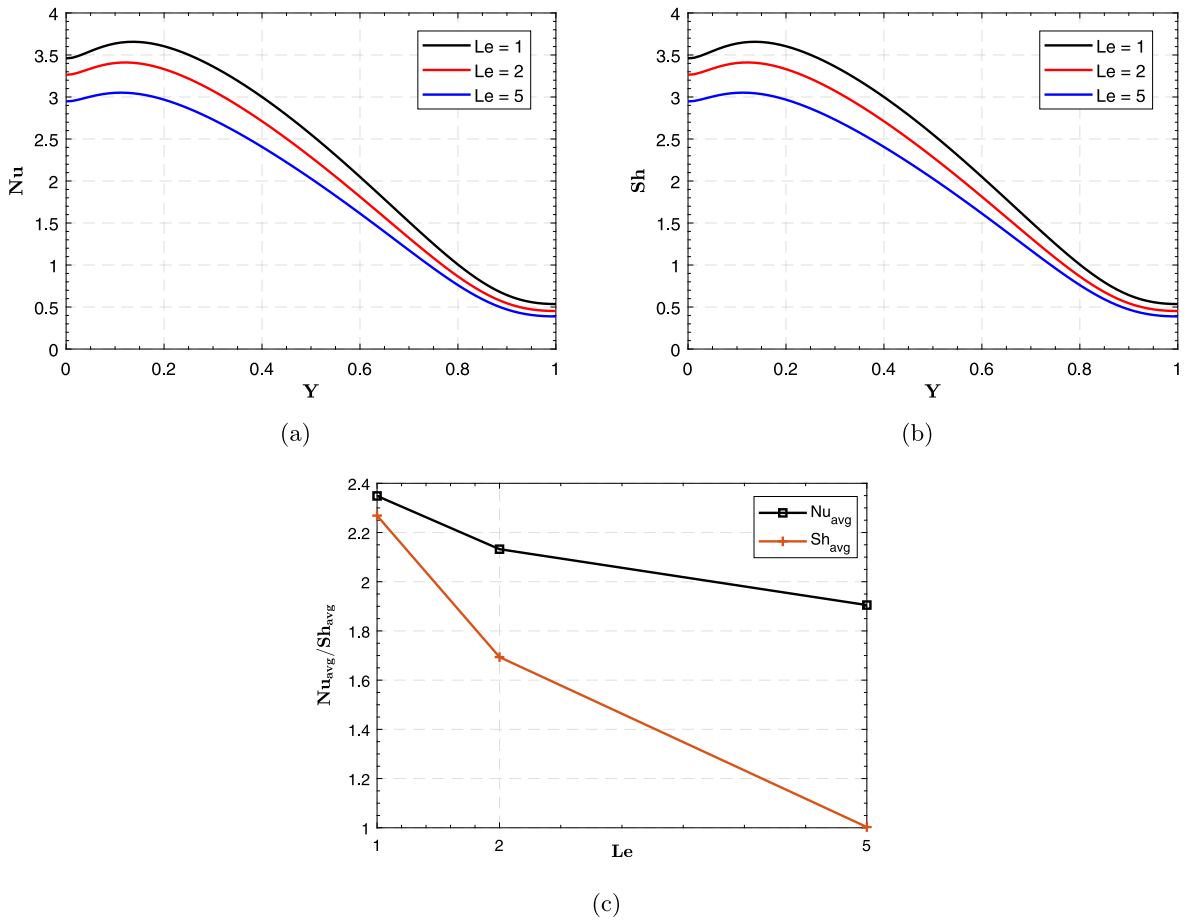

Fig. 14. Comparison of (a) Local Nusselt number, (b) Local Sherwood number, and (c) Average Nusselt and Sherwood number for different Lewis numbers at Ra = 10^4, Pr = 0.71, and N = 1.

At Le = 1, the elliptical type streamlines depict unicellular vortex with value, $\Psi_{min} = -6.278$ at the center of enclosure. The shape of streamlines almost the same with the increase of Lewis number. The magnitude of Ψ_{min} decreases significantly with the increment in Lewis number from Le = 1 to Le = 5, and this indicates that the rate of fluid flow decreases significantly in the enclosure, and hence the rate of flow transfer decreases significantly.

At Le = 1, the $H_{min} = -2.429$ and $M_{min} = -2.489$ and $H_{max} = 2.349$ and $M_{max} = 2.269$, this represents that the pure convection. As Lewis number is augmented from Le = 1 to Le = 5, the magnitude of both, the positive and negative values decreases significantly, and this shows that the direct heat and mass transfer as well as internal transfer decreases significantly. Consequently, the convection rate reduces significantly. The magnitude of H_{min} and H_{max} is almost the same; it shows that the direct heat transfer as well as internal transfer almost same. The magnitude of M_{min} is greater than of M_{max}; this indicates that the internal heat and mass transfer rates dominate the direct heat and mass transfer rates. Furthermore, it can be noticed that the magnitude of H_{min} and H_{max} are greater than the magnitude of M_{min} and M_{max} (except M_{min} at Le = 1), this depicts that the internal as well as the direct heat transfer rates dominate the internal as well as the direct mass transfer rate. However, the magnitude of M_{min} is greater than the magnitude of M_{max}, from this we can notice that the internal mass transfer rate dominates the direct mass transfer rate.

Fig. 13 shows the velocity components, temperature and solute distributions along the horizontal mid of cavity for different Lewis number at Ra = 10^4, Pr = 0.71, and N = 1. When Le increases, both the velocities components are significant decreases, and this indicates that buoyancy forces become weaker than the viscous effects, and hence, convection is dominated by conduction. The distribution of temperature and solute along the horizontal mid of the cavity shows the opposite behavior to each other. Fig. 14 presents the local and average Nusselt and Sherwood numbers along the left wall of the enclosure for different Lewis numbers at Ra = 10^4, Pr = 0.71, and N = 1. At Le = 1, the local Nusselt and Sherwood numbers curve is on top, started from 3.5 and reached to 0.5 while Lewis number augmented the curves are started from 3 and reached to 0.5, and we can say that the convection is dominated by conduction with the increment in Lewis number. Table 7

Table 7
Comparison of velocity, temperature, and solute along the vertical mid of the cavity for different Lewis numbers at Ra = 10^4, Pr = 0.71, and N = 1.

	Le = 1	Le = 2	Le = 5
U_{max}	18.87	15.75	13.40
U_{min}	−18.80	−15.74	−13.39
V_{max}	27.76	24.92	21.68
V_{min}	−27.80	−24.95	−21.30
T_{max}	0.74	0.75	0.76
T_{min}	0.27	0.26	0.26
S_{max}	0.74	0.72	0.66
S_{min}	0.27	0.28	0.30

Table 8
Comparison of average Nusselt and Sherwood numbers for different Lewis numbers at Ra = 10^4, Pr = 0.71, and N = 1.

	Le = 1	Le = 2	Le = 5
Nu_{avg}	2.349	2.132	1.905
Sh_{avg}	2.269	1.694	1.003

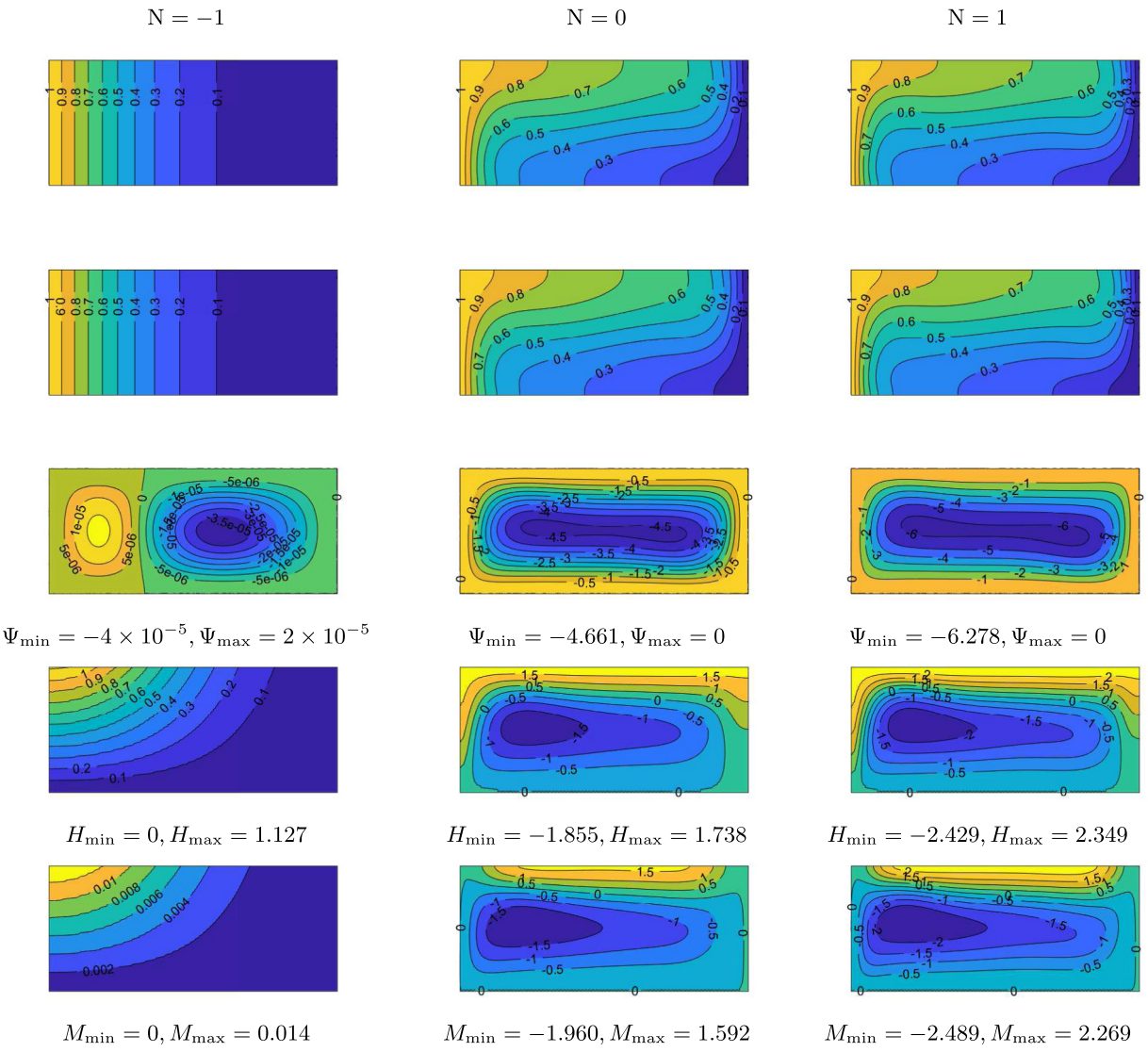

Fig. 15. Isotherms (top row), isosolutes (2rd row), streamlines (3rd row), heatlines (4th row), and masslines (bottom row) for different buoyancy ratios at Ra = 10^4, Pr = 0.71, and Le = 1.

illustrates the maximum and minimum values of horizontal and vertical velocities, temperature and solute along with the vertical mid of the cavity for different Lewis numbers at Ra = 10^4, Pr = 0.71, and N = 1. Fig. 14(c) and Table 8 illustrate that average Nusselt and Sherwood number decreases significantly with the increment in Lewis number. The average Sherwood number decreases more significant than the average Nusselt number, this indicates that the total heat transfer rate dominates the total mass transfer rate.

4.3.4. *Effect of buoyancy ratio on fluid flow, thermal, and solute transfer*

Buoyancy ratio (N) is defined as the ratio of the solute and thermal buoyancy forces. The coefficients of thermal and solute expansions can be either positive or negative, and hence buoyancy ratio can be either positive or negative. Fig. 15 displays the streamlines, isotherms, isosolutes, heatlines, and masslines for different buoyancy ratios at Ra = 10^4, Pr = 0.71, and Le = 1. When N = −1, this indicates that the solute and thermal buoyancy forces are equal but acts in opposite directions. The isotherms are parallel to the sidewalls of the enclosure, and it depicts that the pure conduction process is being happened. The isotherms travel more distance to reach the right wall from the left wall and become more curved when the buoyancy ratio N augmented from −1 to 1, this indicates that the convection process significantly enhanced. Moreover, there is a significant increment in the temperature gradient on the left wall with the increment of the buoyancy ratio. The isosolutes show almost similar patterns when buoyancy ratio augmented and solute gradient increase significantly on the left wall of the enclosure, this indicates that the solute transfer enhanced considerably with the rise in buoyancy ratio N from −1 to 1. At N = −1, there are two circulations are formed; one is in the right part of the enclosure in the anticlockwise direction, and another one is in the right of the enclosure in the clockwise direction. However, $\Psi_{max} = 2 \times 10^{-5}$ and $\Psi_{max} = -4 \times 10^{-5}$ are quite low in fact negligible, this shows that the fluid flow is weak hence conduction is completely dominates the convention. The shape of streamlines becomes elliptical with the increase of buoyancy ratio and the magnitude of the Ψ_{min} augmented significantly; this indicates that the convection is enhanced and maximum convection rate is for N = 1.

At N = −1, the heat and mass lines do not cover the whole enclosure, and the $H_{min} = 0$ and $M_{min} = 0$ and $H_{max} = 1.127$ and $M_{max} = 0.014$, this indicates that there is no internal heat and mass transfer however $H_{max} > M_{max}$, this indicates that the direct heat transfer dominates the direct mass transfer. As buoyancy ratio N augmented, the heat and mass lines cover the whole enclosure, the magnitude of both the positive and negative values are enhanced, and this indicates that the direct heat and mass transfer as well as internal transfer enhanced notably.

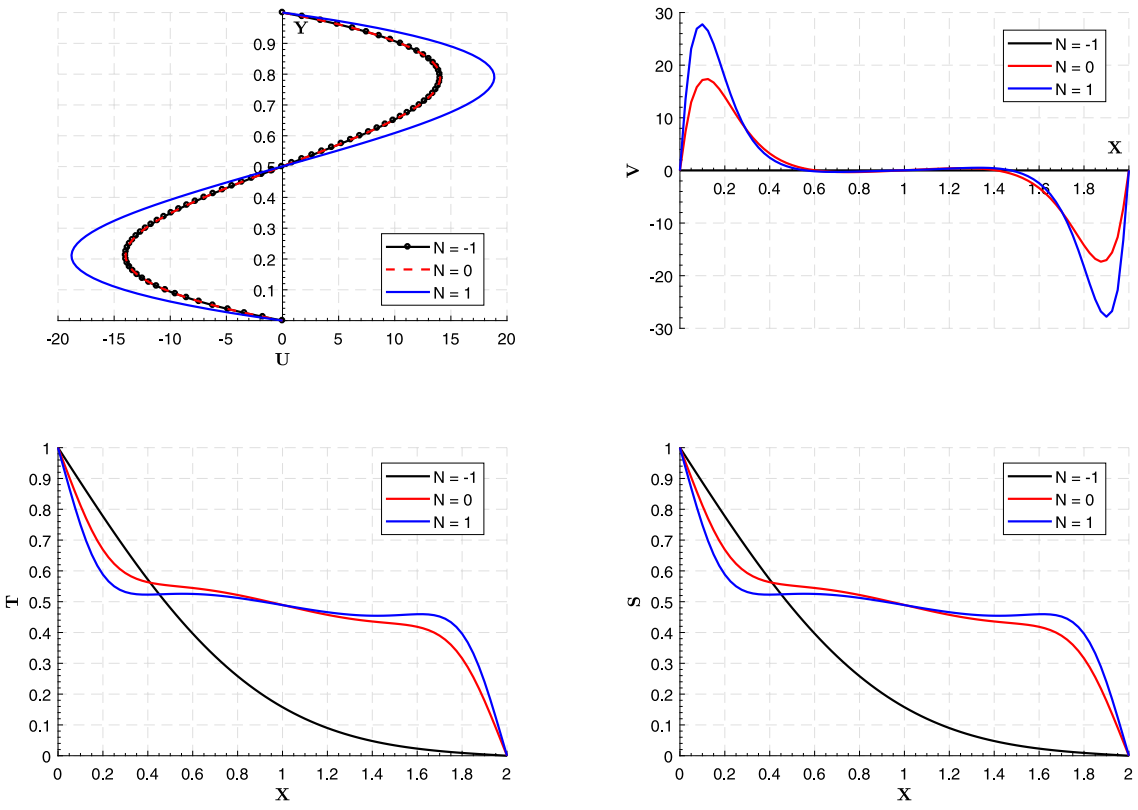

Fig. 16. Variation of velocity, temperature, solute, heat function, mass function, and stream function distributions in the mid of cavity for different buoyancy ratios at Ra = 10^4, Pr = 0.71, and Le = 1.

Table 9
Comparison of velocity, temperature, and solute along the vertical mid of the cavity for different buoyancy ratios at Ra = 10^4, Pr = 0.71, and Le = 1.

	N = −1	N = 0	N = 1
U_{max}	14.05	14.05	18.87
U_{min}	−13.98	−13.98	−18.80
V_{max}	0.00	17.37	27.76
V_{min}	0.00	−17.34	−27.80
T_{max}	0.73	0.73	0.74
T_{min}	0.28	0.28	0.27
S_{max}	0.73	0.73	0.74
S_{min}	0.28	0.28	0.27

Table 10
Comparison of average Nusselt and Sherwood numbers for different buoyancy ratios at Ra = 10^4, Pr = 0.71, and Le = 1.

	N = −1	N = 0	N = 1
Nu_{avg}	1.127	1.738	2.349
Sh_{avg}	0.014	1.592	2.269

Consequently, the convection rate enhances significantly. The internal heat transfer dominates the direct heat transfer as depicted by the magnitude of H_{min} is greater than the magnitude of H_{max}.

Similarly, the internal mass transfer dominates the direct heat transfer. The magnitude of H_{min} and M_{min} is greater than the magnitude of H_{max} and M_{max}, consequently the internal heat and mass transfer rates dominates the direct heat and mass transfer rates. Furthermore, it can be noticed that the magnitude of H_{min} is less than the magnitude of M_{min}; this indicates that the internal mass transfer rate dominates the internal heat transfer rate. However, the magnitude of H_{max} is greater than the magnitude of M_{max}; from this, we can conclude that the direct heat transfer rate dominates the direct mass transfer rate.

Fig. 16 illustrates the velocity components, temperature and solute distributions along the horizontal mid of cavity for different buoyancy ratio at Ra = 10^4, Pr = 0.71, and Le = 1. At N = −1 and N = 0, the horizontal (U-velocity) velocity is identical while for N = 1 it is considerably enhanced. At N = −1, the fluid flow is negligible in the vertical direction of the enclosure, as depicted by the vertical (V-velocity) velocity is zero. When N increases, both the velocities components are significantly increased, and this indicates that buoyancy forces dominate the viscous ones and enhancing the flow convection rate. The distribution of temperature and solute follows a nonlinear profile and enhancing the convention process with the increment in buoyancy ratio. Fig. 17 displays the local and average Nusselt and Sherwood numbers along the left wall of the enclosure for different buoyancy ratio at Ra = 10^4, Pr = 0.71, and Le = 1. At N = −1, the local Nusselt and Sherwood numbers are almost equal to one, and this indicates that the heat transfer occurs due to the pure conduction process. As the buoyancy ratio augmented, the buoyancy forces dominate the viscous effects, and the local Nusselt and Sherwood numbers started from 2.5(N = 0) and 3.5(N = 1) and reached to 0.5 with decreasing manner. Table 9 shows the maximum and minimum values of horizontal and vertical velocities, temperature and solute along with the vertical mid of the cavity for different buoyancy ratios at Ra = 10^4, Pr = 0.71, and Le = 1. Fig. 17(c) and Table 10 show that there is a significant enhancement in average Nusselt and Sherwood number with the increment in buoyancy ratio, however, the total heat transfer rate dominates the total mass transfer rate, this happens because of thermal buoyancy force dominates solute buoyancy force.

5. Conclusions

Thermo-solute natural convection with heat and mass lines in a uniformly heated and soluted rectangular enclosure for low and moderate Prandtl number fluids has been numerically investigated by finite

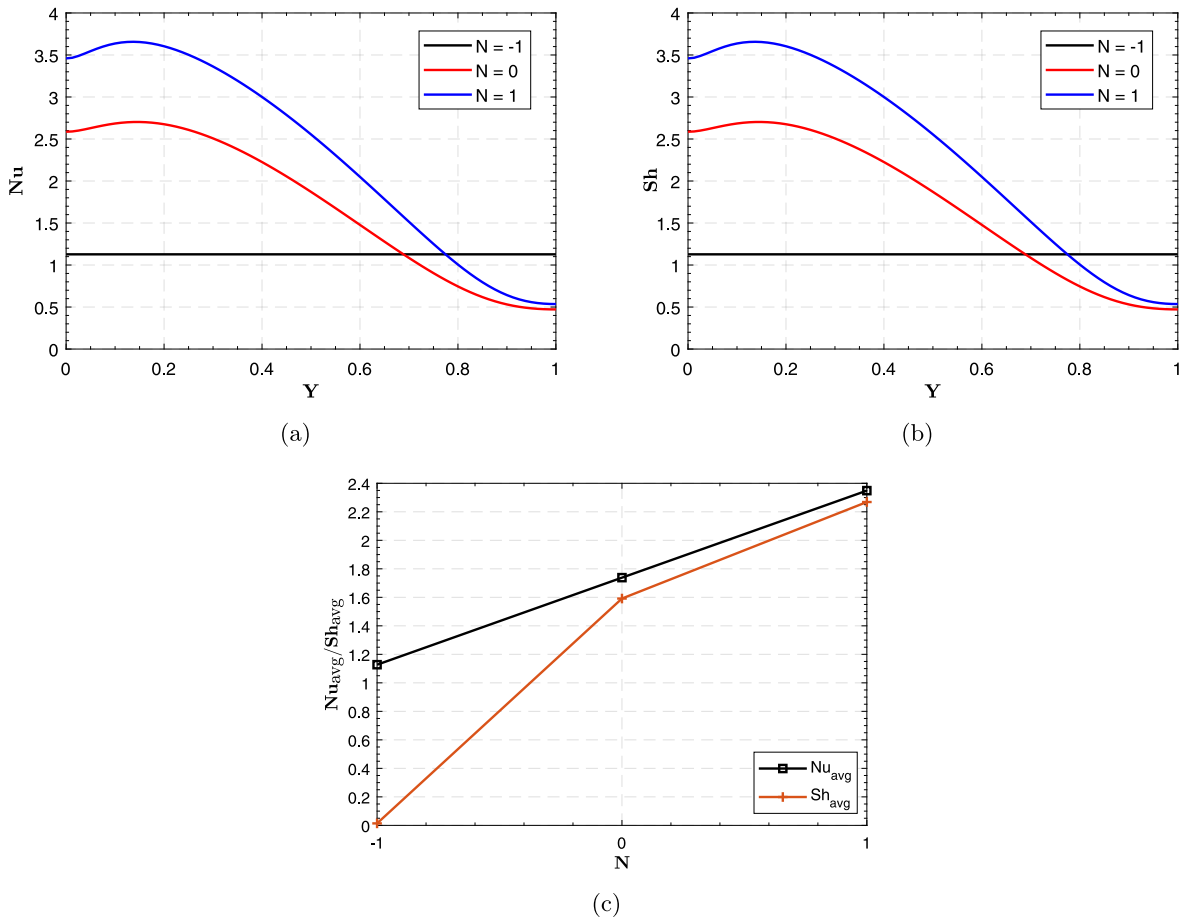

Fig. 17. Comparison of (a) Local Nusselt number, (b) Local Sherwood number, and (c) Average Nusselt and Sherwood number for different buoyancy ratios at Ra = 10^4, Pr = 0.71, and Le = 1.

difference method. The present study has been carried out for the various dependent parameters in the ranges: the Rayleigh number (Ra = $10^3, 10^4, 10^5$), Prandtl number (Pr = $0.015, 0.025, 0.71$), Lewis number (Le = $1, 2, 5$), and buoyancy ratio (N = $-1, 0, 1$), and the streamlines, isotherms, isosolutes, heat, and mass lines along with average Nusselt and Sherwood numbers at the left wall of the enclosure have been displayed graphically for the above mentioned parameters.

- The isotherms and isosolutes give only the temperature and solute along the lines joining the points of equal temperature and solute, respectively. To visualize the heat and solute transfer phenomena inside an enclosure filled with fluids is incomplete unless the path followed by the heat and mass flux is known; for this purpose, the concept of heat and mass function has been introduced. The drawing of isolines of heat and mass functions provide heatlines and masslines.
- The total heat and mass transfer rate are strongly influenced by the Rayleigh number, Prandtl number, Lewis number, and buoyancy ratio, but the heat transfer rate dominates the mass transfer rate.
- As the Ra and Pr augmented, the fluid flow transfer significantly enhanced and maximum for Ra = 10^5 and Pr = 0.71. The internal heat and mass transfer rates, as well as the direct heat and mass transfer rates, notably augmented. The internal heat and mass transfer rates dominate the direct heat and mass transfer rates. Moreover, the internal heat transfer rate is governed by the internal mass transfer rate. Furthermore, the direct heat transfer rate dominates the direct mass transfer rate.
- The fluid flow transfer declined with the increment in the Lewis number and low at Le = 5. The internal heat transfer rate is higher than the direct heat transfer rate for Le = 1. Both internal heat transfer as well as the direct heat transfer rates almost equal as the Lewis number augmented from 2 to 5. The internal mass transfer rate, as well as the direct mass transfer rate, significantly decrease with the augmentation of Lewis number, both are maximum at Le = 1. The internal mass transfer rate dominates the direct mass transfer rate. At Le = 1, the internal mass transfer rate dominates the internal heat transfer rate and the direct mass transfer governed by the direct heat transfer rate. The heat transfer rates dominate mass transfer rates as Le increases from 1 to 5.
- At N = −1, almost negligible fluid flow transfer in the enclosure. The fluid flow transfer significantly enhanced in the enclosure with the increment in the buoyancy ratio. The only direct heat transfer rate for N = −1, whereas both types of mass transfers are negligible. Both the internal heat and mass transfer, as well as the direct heat and mass transfer rates significantly enhanced as the buoyancy ratio augmented from −1 to 1. The internal heat and mass transfer dominate the direct heat and mass transfer. Moreover, the internal heat transfer rate is governed by the internal mass transfer rate; however, the direct heat transfer rate dominates the direct mass transfer rate.

From the detailed analysis of all the considered cases, we can conclude that the heat and mass lines approach play significant roles for the better understanding of energy and solute distributions in the enclosure over isotherms and isosolutes approach.

Declaration of competing interest

The authors declare that they have no known competing financial interests or personal relationships that could have appeared to influence the work reported in this paper.

References

[1] F. Alavyoon, A. Eklund, F. Bark, R. Karlsson, D. Simonsson, Theoretical and experimental studies of free convection and stratification of electrolyte in a lead-acid cell during recharge, Electrochim. Acta 36 (14) (1991) 2153–2164, http://dx.doi.org/10.1016/0013-4686(91)85224-U.

[2] T. Ikeshoji, F.N.B. de Nahui, S. Kimura, M. Yoneya, Computer analysis on natural convection in thin-layer thermocells with a soluble redox couple: Part 2. e-i relation, electric power, heat flux and electrochemical heat pump, J. Electroanal. Chem. Interfacial Electrochem. 312 (1) (1991) 43–56, http://dx.doi.org/10.1016/0022-0728(91)85143-D.

[3] M.M. Rahman, H.F. Öztop, A. Ahsan, M.A. Kalam, Y. Varol, Double-diffusive natural convection in a triangular solar collector, Int. Commun. Heat Mass Transf. 39 (2) (2012) 264–269, http://dx.doi.org/10.1016/j.icheatmasstransfer.2011.11.008.

[4] N. Alleborn, H. Raszillier, F. Durst, Lid-driven cavity with heat and mass transport, Int. J. Heat Mass Transfer 42 (5) (1999) 833–853, http://dx.doi.org/10.1016/S0017-9310(98)00224-5.

[5] S.E. Zorrilla, A.C. Rubiolo, Mathematical modeling for immersion chilling and freezing of foods: Part I: Model development, J. Food Eng. 66 (3) (2005) 329–338, http://dx.doi.org/10.1016/j.jfoodeng.2004.03.026.

[6] S.-i. Niwa, M. Eswaramoorthy, J. Nair, A. Raj, N. Itoh, H. Shoji, T. Namba, F. Mizukami, A one-step conversion of benzene to phenol with a palladium membrane, Science 295 (5552) (2002) 105–107, http://dx.doi.org/10.1126/science.1066527.

[7] L.B. Snoussi, R. Chouikh, A. Guizani, Numerical study of the natural convection flow resulting from the combined buoyancy effects of thermal and mass diffusion in a cavity with differentially heated side walls, Desalination 182 (1–3) (2005) 143–150, http://dx.doi.org/10.1016/j.desal.2005.03.014.

[8] H.S. Harzallah, A. Jbara, K. Slimi, Double-diffusive natural convection in anisotropic porous medium bounded by finite thickness walls: Validity of local thermal equilibrium assumption, Transp. Porous Media 103 (2) (2014) 207–231, http://dx.doi.org/10.1007/s11242-014-0298-3.

[9] D.W. Crunkleton, R. Narayanan, T.J. Anderson, Numerical simulations of periodic flow oscillations in low prandtl number fluids, Int. J. Heat Mass Transfer 49 (1) (2006) 427–438, http://dx.doi.org/10.1016/j.ijheatmasstransfer.2004.09.009.

[10] L. Zhang, Y.-R. Li, C.-M. Wu, Effect of surface heat dissipation on thermocapillary convection of low prandtl number fluid in a shallow annular pool, Int. J. Heat Mass Transfer 110 (2017) 460–466, http://dx.doi.org/10.1016/j.ijheatmasstransfer.2017.03.059.

[11] L. Zhang, Y.-R. Li, C.-M. Wu, Q.-S. Liu, Flow pattern transition and destabilization mechanism of thermocapillary convection for low prandtl number fluid in a deep annular pool with surface heat dissipation, Int. J. Heat Mass Transfer 126 (2018) 118–127, http://dx.doi.org/10.1016/j.ijheatmasstransfer.2018.05.120.

[12] L. Zhang, Y.-R. Li, C.-M. Wu, Q.-S. Liu, Flow bifurcation routes to chaos of thermocapillary convection for low prandtl number fluid in shallow annular pool with surface heat dissipation, Int. J. Therm. Sci. 125 (2018) 23–33, http://dx.doi.org/10.1016/j.ijthermalsci.2017.11.010.

[13] X. Xu, Z.-T. Yu, Y.-C. Hu, L.-W. Fan, K.-F. Cen, Transient natural convective heat transfer of a low-prandtl-number fluid from a heated horizontal circular cylinder to its coaxial triangular enclosure, Int. J. Heat Mass Transfer 55 (4) (2012) 995–1003, http://dx.doi.org/10.1016/j.ijheatmasstransfer.2011.10.011.

[14] Z.-T. Yu, X. Xu, Y.-C. Hu, L.-W. Fan, K.-F. Cen, Transient natural convective heat transfer of a low-prandtl-number fluid inside a horizontal circular cylinder with an inner coaxial triangular cylinder, Int. J. Heat Mass Transfer 53 (23) (2010) 5102–5110, http://dx.doi.org/10.1016/j.ijheatmasstransfer.2010.06.056.

[15] T. Zürner, F. Schindler, T. Vogt, S. Eckert, J. Schumacher, Combined measurement of velocity and temperature in liquid metal convection, J. Fluid Mech. 876 (2019) 1108–1128, http://dx.doi.org/10.1017/jfm.2019.556.

[16] J. Oder, A. Shams, L. Cizelj, I. Tiselj, Direct numerical simulation of low-prandtl fluid flow over a confined backward facing step, Int. J. Heat Mass Transfer 142 (2019) 118436, http://dx.doi.org/10.1016/j.ijheatmasstransfer.2019.118436.

[17] S. Saravanan, P. Kandaswamy, Buoyancy convection in low prandtl number liquids with large temperature variation, Meccanica 37 (6) (2002) 599–608, http://dx.doi.org/10.1023/A:1020959623479.

[18] P. Deshmukh, S.K. Mitra, U.N. Gaitonde, Investigation of natural circulation in cavities with uniform heat generation for different prandtl number fluids, Int. J. Heat Mass Transfer 54 (7–8) (2011) 1465–1474, http://dx.doi.org/10.1016/j.ijheatmasstransfer.2010.11.046.

[19] L. Zhang, Y.-R. Li, H. Zhang, Onset of double-diffusive Rayleigh-Bénard convection of a moderate Prandtl number binary mixture in cylindrical enclosures, Int. J. Heat Mass Transfer 107 (2017) 500–509, http://dx.doi.org/10.1016/j.ijheatmasstransfer.2016.11.054.

[20] K.-Q. Ma, J. Liu, Heat-driven liquid metal cooling device for the thermal management of a computer chip, J. Phys. D: Appl. Phys. 40 (15) (2007) 4722–4729, http://dx.doi.org/10.1088/0022-3727/40/15/055.

[21] H. Ge, H. Li, S. Mei, J. Liu, Low melting point liquid metal as a new class of phase change material: An emerging frontier in energy area, Renew. Sustain. Energy Rev. 21 (2013) 331–346, http://dx.doi.org/10.1016/j.rser.2013.01.008.

[22] T. Nishimura, M. Wakamatsu, A.M. Morega, Oscillatory double-diffusive convection in a rectangular enclosure with combined horizontal temperature and concentration gradients, Int. J. Heat Mass Transfer 41 (11) (1998) 1601–1611, http://dx.doi.org/10.1016/S0017-9310(97)00271-8.

[23] E. Papanicolaou, V. Belessiotis, Double-diffusive natural convection in an asymmetric trapezoidal enclosure: Unsteady behavior in the laminar and the turbulent-flow regime, Int. J. Heat Mass Transfer 48 (1) (2005) 191–209, http://dx.doi.org/10.1016/j.ijheatmasstransfer.2004.07.040.

[24] N. Nithyadevi, R.J. Yang, Double diffusive natural convection in a partially heated enclosure with soret and dufour effects, Int. J. Heat Fluid Flow 30 (5) (2009) 902–910, http://dx.doi.org/10.1016/j.ijheatfluidflow.2009.04.001.

[25] S. Chen, J. Tölke, M. Krafczyk, Numerical investigation of double-diffusive (natural) convection in vertical annuluses with opposing temperature and concentration gradients, Int. J. Heat Fluid Flow 31 (2) (2010) 217–226, http://dx.doi.org/10.1016/j.ijheatfluidflow.2009.12.013.

[26] M. Hasanuzzaman, M.M. Rahman, H.F. Öztop, N.A. Rahim, R. Saidur, Effects of lewis number on heat and mass transfer in a triangular cavity, Int. Commun. Heat Mass Transf. 39 (8) (2012) 1213–1219, http://dx.doi.org/10.1016/j.icheatmasstransfer.2012.07.002.

[27] F. Oueslati, B. Ben-Beya, T. Lili, Double-diffusive natural convection and entropy generation in an enclosure of aspect ratio 4 with partial vertical heating and salting sources, Alexandria Eng. J. 52 (2013) 605–625, http://dx.doi.org/10.1016/j.aej.2013.09.006.

[28] M.B. Uddin, M. Rahman, M. Khan, T.A. Ibrahim, Effect of buoyancy ratio on unsteady thermosolutal combined convection in a lid driven trapezoidal enclosure in the presence of magnetic field, Comput. & Fluids 114 (2015) 284–296, http://dx.doi.org/10.1016/j.compfluid.2015.03.017.

[29] M. Corcione, S. Grignaffini, A. Quintino, Correlations for the double-diffusive natural convection in square enclosures induced by opposite temperature and concentration gradients, Int. J. Heat Mass Transfer 81 (2015) 811–819, http://dx.doi.org/10.1016/j.ijheatmasstransfer.2014.11.013.

[30] C. Ren, Y. Wan, A new approach to the analysis of heat and mass transfer characteristics for laminar air flow inside vertical plate channels with falling water film evaporation, Int. J. Heat Mass Transfer 103 (2016) 1017–1028, http://dx.doi.org/10.1016/j.ijheatmasstransfer.2016.07.109.

[31] J. Wang, M. Yang, Y.L. He, Y. Zhang, Oscillatory double-diffusive convection in a horizontal cavity with soret and dufour effects, Int. J. Therm. Sci. 106 (2016) 57–69, http://dx.doi.org/10.1016/j.ijthermalsci.2016.03.012.

[32] A. Ja, A. Cheddadi, Numerical investigation of buoyancy balance effect on thermosolutal convection in a horizontal annular porous cavity, Eur. Phys. J. E 42 (1) (2019) 9, http://dx.doi.org/10.1140/epje/i2019-11768-0.

[33] M.A. Sheremet, The influence of cross effects on the characteristics of heat and mass transfer in the conditions of conjugate natural convection, J. Eng. Thermophys. 19 (3) (2010) 119–127, http://dx.doi.org/10.1134/S1810232810030021.

[34] T. Groşan, M.A. Sheremet, I. Pop, S.R. Pop, Double-diffusive natural convection in a differentially heated wavy cavity under thermophoresis effect, J. Thermophys. Heat Transfer 32 (4) (2018) 1045–1058, http://dx.doi.org/10.2514/1.T5389.

[35] G. Kuznetsov, M. Sheremet, Conjugate heat transfer in an enclosure under the condition of internal mass transfer and in the presence of the local heat source, Int. J. Heat Mass Transfer 52 (1) (2009) 1–8, http://dx.doi.org/10.1016/j.ijheatmasstransfer.2008.06.034.

[36] G.V. Kuznetsov, M.A. Sheremet, A numerical simulation of double-diffusive conjugate natural convection in an enclosure, Int. J. Therm. Sci. 50 (10) (2011) 1878–1886, http://dx.doi.org/10.1016/j.ijthermalsci.2011.05.003.

[37] T. Bao, Z.L. Liu, Thermohaline stratification modeling in mine water via double-diffusive convection for geothermal energy recovery from flooded mines, Appl. Energy 237 (2019) 566–580, http://dx.doi.org/10.1016/j.apenergy.2019.01.049.

[38] S. Kimura, A. Bejan, The heatline visualization of convective heat transfer, J. Heat Transfer 105 (November 1983) (1983) 916–919.

[39] V. Costa, Double diffusive natural convection in a square enclosure with heat and mass diffusive walls, Int. J. Heat Mass Transfer 40 (17) (1997) 4061–4071, http://dx.doi.org/10.1016/S0017-9310(97)00061-6.

[40] M.M. Rahman, H.F. Öztop, S. Mekhilef, R. Saidur, J. Orfi, Simulation of unsteady heat and mass transport with heatline and massline in a partially heated open cavity, Appl. Math. Model. 39 (5–6) (2015) 1597–1615, http://dx.doi.org/10.1016/j.apm.2014.09.022.

[41] S.H. Hussain, Analysis of heatlines and entropy generation during double-diffusive MHD natural convection within a tilted sinusoidal corrugated porous enclosure, Eng. Sci. Technol. Int. J. 19 (2016) 926–945, http://dx.doi.org/10.1016/j.jestch.2015.12.001.

[42] A.I. Alsabery, A.J. Chamkha, H. Saleh, I. Hashim, Heatline visualization of conjugate natural convection in a square cavity filled with nanofluid with sinusoidal temperature variations on both horizontal walls, Int. J. Heat Mass Transfer 100 (2016) 835–850, http://dx.doi.org/10.1016/j.ijheatmasstransfer.2016.05.031.

[43] J.T. Hu, X.H. Ren, D. Liu, F.Y. Zhao, H.Q. Wang, Natural convective heat and moisture transfer in an inclined building enclosure with one slender wall of finite thickness: Analytical investigation and non-unique steady flow solutions, Int. J. Heat Mass Transfer 104 (2017) 1160–1176, http://dx.doi.org/10.1016/j.ijheatmasstransfer.2016.09.033.

[44] N.S. Bondareva, M.A. Sheremet, H.F. Oztop, N. Abu-Hamdeh, Heatline visualization of natural convection in a thick walled open cavity filled with a nanofluid, Int. J. Heat Mass Transfer 109 (2017) 175–186, http://dx.doi.org/10.1016/j.ijheatmasstransfer.2017.01.124.

[45] V. Kishor, S. Singh, A. Srivastava, Investigation of convective heat transfer phenomena in differentially-heated vertical closed cavity: Whole field experiments and numerical simulations, Exp. Therm Fluid Sci. 99 (2018) 71–84, http://dx.doi.org/10.1016/j.expthermflusci.2018.07.021.

[46] H. Han, T.H. Kuehn, Double diffusive natural convection in a vertical rectangular enclosure—II. Numerical study, Int. J. Heat Mass Transfer 34 (2) (1991) 461–471, http://dx.doi.org/10.1016/0017-9310(91)90265-G.

[47] F.Y. Zhao, D. Liu, G.F. Tang, Application issues of the streamline, heatline and massline for conjugate heat and mass transfer, Int. J. Heat Mass Transfer 50 (1–2) (2007) 320–334, http://dx.doi.org/10.1016/j.ijheatmasstransfer.2006.06.026.

[48] H.F. Oztop, E. Abu-Nada, Numerical study of natural convection in partially heated rectangular enclosures filled with nanofluids, Int. J. Heat Fluid Flow 29 (5) (2008) 1326–1336, http://dx.doi.org/10.1016/j.ijheatfluidflow.2008.04.009.

[49] D.S. Bondarenko, M.A. Sheremet, H.F. Oztop, M.E. Ali, Natural convection of al2o3/h2o nanofluid in a cavity with a heat-generating element. heatline visualization, Int. J. Heat Mass Transfer 130 (2019) 564–574, http://dx.doi.org/10.1016/j.ijheatmasstransfer.2018.10.091.

[50] O. Trevisan, A. Bejan, Combined heat and mass transfer by natural convection in a vertical enclosure, J. Heat Transfer 109 (1) (1987) 104–112, http://dx.doi.org/10.1016/S0065-2717(08)70029-7.

[51] G. De Vahl Davis, I.P. Jones, Natural convection in a square cavity: A comparison exercise, Internat. J. Numer. Methods Fluids 3 (3) (1983) 227–248, http://dx.doi.org/10.1002/fld.1650030304.

[52] N. Markatos, K. Pericleous, Laminar and turbulent natural convection in an enclosed cavity, Int. J. Heat Mass Transfer 27 (5) (1984) 755–772, http://dx.doi.org/10.1016/0017-9310(84)90145-5.

[53] K. Khanafer, K. Vafai, M. Lightstone, Buoyancy-driven heat transfer enhancement in a two-dimensional enclosure utilizing nanofluids, Int. J. Heat Mass Transfer 46 (19) (2003) 3639–3653, http://dx.doi.org/10.1016/S0017-9310(03)00156-X.

[54] R.K. Tiwari, M.K. Das, Heat transfer augmentation in a two-sided lid-driven differentially heated square cavity utilizing nanofluids, Int. J. Heat Mass Transfer 50 (9) (2007) 2002–2018, http://dx.doi.org/10.1016/j.ijheatmasstransfer.2006.09.034.

[55] L.C. Woods, A note on the numerical solution of fourth order differential equations, Aeronaut. Q. 5 (4) (1954) 176–184, http://dx.doi.org/10.1017/S0001925900001177.